Targeted Reactivation of *FMR1* Transcription in Fragile X Syndrome Embryonic Stem Cells

Jill M. Haenfler[1,2†], Geena Skariah[1†], Caitlin M. Rodriguez[1], Andre Monteiro da Rocha[3], Jack M. Parent[1,4], Gary D. Smith[5] and Peter K. Todd[1,4]*

[1]*Department of Neurology, University of Michigan, Ann Arbor, MI, United States,* [2]*Department of Molecular, Cellular and Developmental Biology, University of Michigan, Ann Arbor, MI, United States,* [3]*Department of Internal Medicine, Center for Arrhythmia Research, University of Michigan, Ann Arbor, MI, United States,* [4]*Veterans Administration Ann Arbor Healthcare System, Ann Arbor, MI, United States,* [5]*Departments of Obstetrics/Gynecology, Physiology, and Urology, University of Michigan, Ann Arbor, MI, United States*

Fragile X Syndrome (FXS) is the most common inherited cause of intellectual disability and autism. It results from expansion of a CGG nucleotide repeat in the 5′ untranslated region (UTR) of *FMR1*. Large expansions elicit repeat and promoter hyper-methylation, heterochromatin formation, *FMR1* transcriptional silencing and loss of the Fragile X protein, FMRP. Efforts aimed at correcting the sequelae resultant from FMRP loss have thus far proven insufficient, perhaps because of FMRP's pleiotropic functions. As the repeats do not disrupt the FMRP coding sequence, reactivation of endogenous *FMR1* gene expression could correct the proximal event in FXS pathogenesis. Here we utilize the Clustered Regularly Interspaced Palindromic Repeats/deficient CRISPR associated protein 9 (CRISPR/dCas9) system to selectively re-activate transcription from the silenced *FMR1* locus. Fusion of the transcriptional activator VP192 to dCas9 robustly enhances *FMR1* transcription and increases FMRP levels when targeted directly to the CGG repeat in human cells. Using a previously uncharacterized FXS human embryonic stem cell (hESC) line which acquires transcriptional silencing with serial passaging, we achieved locus-specific transcriptional re-activation of *FMR1* messenger RNA (mRNA) expression despite promoter and repeat methylation. However, these changes at the transcript level were not coupled with a significant elevation in FMRP protein expression in FXS cells. These studies demonstrate that directing a transcriptional activator to CGG repeats is sufficient to selectively reactivate *FMR1* mRNA expression in Fragile X patient stem cells.

Keywords: Fragile X Syndrome, human embryonic stem cells, CRISPR-dCas9, transcriptional activation, VP-192, nucleotide repeat expansion

INTRODUCTION

Fragile X Syndrome (FXS) is an X-linked disorder affecting approximately 1 in 4,000 males and 1 in 8,000 females worldwide (Tassone et al., 2012; Hunter et al., 2014). It is the leading inherited cause of intellectual disability and autism. Many FXS patients also experience attention deficit hyperactivity disorder (ADHD), increased seizure susceptibility, anxiety and language difficulties. FXS results from expansion of a CGG trinucleotide repeat within the 5′ untranslated region (UTR) of the fragile X gene, *FMR1*. Normally, *FMR1* has between 25 and 40 CGG repeats.

Instability of the CGG repeat over multiple generations leads to large (>200) expansions that markedly alter the epigenetic profile of the *FMR1* locus (reviewed in Usdin and Kumari, 2015). In most FXS patients, both the CGG repeat and the *FMR1* promoter are hypermethylated at cytosine residues (Oberlé et al., 1991; Pieretti et al., 1991). This hypermethylation is associated with epigenetic marks consistent with heterochromatin formation over the locus and a partial or complete loss of *FMR1* messenger RNA (mRNA) transcription (Coffee et al., 2002). Although the exact mechanism and order of events leading to transcriptional silencing remains incompletely understood, the net result of these epigenetic alterations is the absence of the Fragile X Mental Retardation Protein, FMRP.

There is strong evidence that loss of FMRP causes FXS symptoms, as rare patients with mutations or deletions elsewhere in *FMR1* also present with FXS (Gedeon et al., 1992; De Boulle et al., 1993; Bhakar et al., 2012; Santoro et al., 2012). Moreover, *Fmr1* knockout (KO) mouse models recapitulate many key features of the human disease, including learning deficits, abnormal socialization and anxiety behaviors, enhanced seizure susceptibility and dendritic spine morphologic abnormalities (Bhakar et al., 2012; Santoro et al., 2012). FMRP is an RNA-binding protein that binds ∼4% of brain mRNAs, including an enriched fraction of synaptic transcripts from genes associated with autism (Brown et al., 2001; Darnell et al., 2011; Ascano et al., 2012). FMRP regulates activity-dependent protein translation at synapses (Bhakar et al., 2012), where it suppresses translation of bound transcripts, either through direct interactions or via association with translating ribosomes (Feng et al., 1997; Darnell et al., 2011; Chen et al., 2014). Upon activation of Group 1 metabotropic glutamate receptors (mGluRs), FMRP is dephosphorylated and rapidly degraded, allowing for local translation of FMRP-associated mRNAs (Ceman et al., 2003; Hou et al., 2006; Nalavadi et al., 2012).

Dysregulation of mGluR signaling is thought to play a central role in disease pathogenesis, and both genetic and pharmacologic targeting of these receptors suppresses phenotypes in mice (Bear et al., 2004; Dölen et al., 2007; Michalon et al., 2012). However, studies of mGluR inhibitors in humans were unsuccessful (Berry-Kravis et al., 2016; Berry-Kravis E. M. et al., 2017). Other preclinical studies in *Fmr1* KO mice and *Drosophila* models demonstrated dysfunction in GABAergic signaling (Chang et al., 2008; Braat et al., 2015). This too led to a series of clinical trials that failed to meet their primary endpoint (Berry-Kravis E. et al., 2017; Berry-Kravis E. M. et al., 2017; Ligsay et al., 2017). More recently, FMRP was found to have additional functions in targeting of ion channel proteins in neurons through direct protein-protein interactions, and these functions underlie some of the phenotypic and electrophysiological abnormalities in *Fmr1* KO mice (Brown et al., 2010; Lee et al., 2011; Deng et al., 2013). FMRP also functions as part of the RNA Induced Silencing Complex (RISC) complex in microRNA translational silencing and has poorly understood nuclear functions which may be relevant to disease phenotypes (Cheever and Ceman, 2009; Kim et al., 2009; Alpatov et al., 2014; Korb et al., 2017). Thus, one potential explanation for the lack of success in human clinical trials to date is that

the pleiotropic functions played by FMRP in neurons and other cell types may be difficult to correct with any treatment targeting only one dysregulated pathway (Berry-Kravis E. M. et al., 2017).

An alternative approach to therapeutic development in FXS involves directly targeting the proximal event in disease pathogenesis—the transcriptional silencing of the *FMR1* gene (Tabolacci et al., 2016). While most FXS patients exhibit CGG repeat methylation, in a fraction of cases this methylation is incomplete or absent, allowing for continued *FMR1* transcription (Nolin et al., 1994; Jacquemont et al., 2011). However, large transcribed repeats still exhibit marked translational inefficiency, presumably due to the repeat element precluding ribosomal scanning through the start codon utilized to generate FMRP (Feng et al., 1995). Despite this, in cases where some *FMR1* transcription occurs, expression correlates with both symptom severity and response to therapeutics (Tassone et al., 1999; Jacquemont et al., 2011). These findings suggest that even small changes in *FMR1* mRNA expression might lead to phenotypic improvements in patients.

Previous work utilizing pharmacological approaches to reactivation of the *FMR1* locus met with some success. Application of non-specific demethylating agents such as 5-azadeoxycytidine (5-azadC) to Fragile X patient derived cells is sufficient to at least transiently enhance *FMR1* transcription and in some cases recover FMRP expression (Chiurazzi et al., 1998). Similarly, treatment with agents that alter the epigenetic landscape, such as the SIRT1 histone deacetylase inhibitor splitomycin, can also re-activate *FMR1* transcription in patient-derived lymphoblastoid cell lines, suggesting that other epigenetic manipulations may also be effective (Biacsi et al., 2008). Approaches coupling these two techniques hold promise at extending the potential effects in patient cells (Kumari and Usdin, 2016). However, many of these agents are toxic in humans and have the potential for significant off-target activity elsewhere in the genome, potentially confounding their use clinically in FXS patients.

An important step in developing methods for reactivation of *FMR1* transcription is identifying a model that demonstrates the developmental epigenetic silencing that occurs in FXS patients. Human embryonic stem cells (hESCs) are important disease models for studying developmental processes for which no other suitable models exist. Previous studies in FXS hESC show that some full mutation hESC remain unmethylated following derivation and exhibit gradual loss of *FMR1* mRNA during directed neuronal differentiation (Eiges et al., 2007; Telias et al., 2013; Colak et al., 2014), similar to the silencing observed in human FXS fetuses (Malter et al., 1997). In other lines, however, gene silencing occurs absent differentiation and appears to be repeat-length dependent, with expansions beyond 400 repeats demonstrating greater silencing (Avitzour et al., 2014; Brykczynska et al., 2016; Zhou et al., 2016). However, many hESC lines derived and characterized to date are not currently available in the United States for federally funded research.

More recently, researchers have taken a more targeted approach to *FMR1* gene reactivation using the Clustered

Regularly Interspaced Palindromic Repeats-CRISPR associated protein 9 (CRISPR-Cas9) system (Doudna and Charpentier, 2014). This technique utilizes either one or a set of single guide RNAs (sgRNAs) to target the CRISPR-Cas9 complex to specific genomic loci. The Cas9 endonuclease then nicks the DNA, allowing for either introduction of a deletion or for homology-directed repair. Two separate groups have now utilized CRISPR-Cas9 to delete expanded CGG repeats in Fragile X patient derived cells (Park et al., 2016; Xie et al., 2016). In both cases, removal of the repeat led to reactivation of the *FMR1* gene and production of FMRP.

In addition to endonuclease-mediated gene editing, the CRISPR-Cas9 system can also be modified to allow for targeted gene expression modulation in multiple systems (Hsu et al., 2014). Of particular interest is the use of CRISPR-Cas9 to activate gene expression by using an endonuclease-deficient Cas9 (dCas9) fused to a transcriptional activator (Perez-Pinera et al., 2013). Here, we show evidence for the targeted activation of the *FMR1* gene using a dCas9 fused to multiple domains of the VP16 transcriptional activator. Our initial studies in cell lines show differential activity for the various dCas9-VP16 fusion constructs with the most robust activity seen with the dCas9-VP192 construct. This system was used in a newly characterized hESC line derived from a Preimplantation Genetic Diagnosis (PGD) FXS embryo. The FXS hESCs show a passage-dependent silencing of the *FMR1* transcript. The dCas9-VP192 construct coupled with guide RNAs targeting the CGG repeat elicited significant activation of *FMR1* transcription in both the early and late passage FXS hESCs and in patient derived Neural Progenitor Cells (NPCs). Overall, these data provide proof-of-principle evidence that CRISPR-dCas9 based transcriptional activation approaches can reactivate *FMR1* transcription even in the setting of large methylated repeats. Targeting the repeat itself may enhance such efforts by providing multiple sequential binding sites for sgRNAs, effectively leveraging the disease mutation to greater efficacy.

MATERIALS AND METHODS

CRISPR Guide RNA Design and Plasmids

Promoter-targeted gRNA sequences were identified within 500 nucleotides upstream of the main transcriptional start site based on the prediction of on-target to off-target effect in the human genome and arrangement within the region using the CRISPR design web portal (Hsu et al., 2013). These sequences and the CGG repeat sequence were cloned into the pSPgRNA plasmid by replacing the sequence between the BbsI sites using the Q5 site-directed mutagenesis kit (NEB) and the primers listed in **Supplementary Table S1**. All dCas9 expression plasmids were obtained from Addgene. pcDNA-dCas9-VP64, pSPgRNA and pLV hUbC-dCas9 VP64-T2A-GFP were gifts from Charles Gersbach (Addgene plasmid # 47107, 47108, 53192, respectively; Perez-Pinera et al., 2013). SP-dCas9-VPR was a gift from George Church (Addgene plasmid # 63798; Chavez et al., 2015). pAC93-pmax-dCas9VP160 was a gift from Rudolf Jaenisch (Addgene plasmid # 48225; Cheng

et al., 2013). pCXLE-dCas9VP192-T2A-EGFP was a gift from Timo Otonkoski (Addgene plasmid # 69536; Balboa et al., 2015). pcDNA3.1(+) and pEGFP-N1 served as control plasmids.

Cell Culture and Transfection of HEK293T Cells

HEK293T cells (ATCC) were maintained at 37°C, 5% CO_2 in Dulbecco's modified Eagle's Medium supplemented with 10% FBS, 100 U/mL penicillin and 100 μg/mL streptomycin following standard procedures. Transfections were performed using Lipofectamine 3000 transfection reagent (Invitrogen) according to manufacturer's instructions. Transfection efficiencies were typically 80%, as determined by fluorescence microscopy after delivery of a control eGFP expression plasmid, and only samples with transfection efficiencies in this range were utilized for further experiments. dCas9 expression plasmids were transfected at a mass ratio of 3:1 to either the CGG gRNA expression plasmid or the identical amount of gRNA expression plasmid consisting of a mixture of equal amounts of the four promoter-targeted gRNAs. Cells were harvested 48 h after transfection.

RNA Isolation and Quantitative RT-PCR

Total RNA was isolated using the Quick RNA Miniprep kit (Zymo research) with on-column DNase I treatment followed by cDNA synthesis using the iScript Reverse Transcriptase kit (Biorad) according to the manufacturer's protocol. Quantitative RT-PCR was performed on the Bio-Rad iCycler real-time detection system using the iQ SYBR Green Supermix (Biorad) and the primers (IDT) listed in **Supplementary Table S1**. Primer specificity was confirmed by gel electrophoresis and melting curve analysis. Relative fold expression for genes of interest was calculated using the comparative CT method (Schmittgen and Livak) with HPRT as the internal control. Technical triplicates were averaged and recorded for each sample. To identify potential off-target genes, a blast search of the human transcriptome was performed with a sequence of 10 CGG repeats (30 nucleotides). The hits were sorted based on their total score. Primers for qPCR were designed for all genes with a score greater than or equal to *FMR1*. All of these genes contained repeats in the 5′UTR similar to *FMR1*.

Western Blot

Cells were washed with cold PBS and lysed on ice in RIPA buffer (50 mM Tris-Cl pH-8.0, 150 mM NaCl, 0.1% SDS, 0.1% Sodium deoxycholate, 1% NP-40) with complete protease inhibitor cocktail (Roche). Samples were centrifuged at 14,000 RPM for 5 min at 4°C and supernatant was transferred to a clean tube. For western blot, protein lysates were boiled in Laemelli buffer and separated on SDS-PAGE gels. Gels were transferred to PVDF membranes, blocked with 5% nonfat dry milk and probed with mouse anti-FMRP (6B8; Biolegend 834601), rabbit anti-Cas9 (Clontech 632607) and rat anti-tubulin (Abcam ab-6160) primary antibodies. Secondary antibodies were goat anti-mouse HRP (Jackson Immunoresearch), IRDye

800 goat anti-rabbit IgG (LI-COR) and IRDye 800 goat anti-rat IgG (LI-COR), respectively. Antibodies were detected using an Odyssey imager or using Western Lightning Plus-ECL substrate (Perkin-Elmer) and developed on film. Quantification of western blot signal were performed as previously described (Renoux et al., 2014). ImageJ was used for quantification. Band intensity was confirmed to be in the linear range by densitometry measurements on control samples with 0.5× or 2× the amount of protein on left edge of blot. Experiments were performed in technical triplicate, and FMRP/tubulin ratio was determined for each sample. These ratios were averaged, normalized to the mean control value for each experiment, and expressed as % control. As multiple groups were compared simultaneously, a Kruskal-Wallis one-way ANOVA was used with Dunn's multiple comparison test applied to account for repeated measures.

Immunocytochemistry

Cells were cultured in chamber slides or on coverslips. The media was removed and cells were washed with 1× PBS and fixed in 4% PFA/4% Sucrose solution for 15 min at room temperature (RT). The cells were permeabilized with 0.1% Triton X-100 for 5 min at RT and were blocked in a 5% Normal Goat Serum solution for 1 h at RT. The cells were stained with primary antibodies overnight at 4°C followed by three washes in 1× PBS for 5 min each. The antibodies used were: mouse anti-FMRP (6B8) at 1:250 dilution (Biolegend 834601), rabbit anti-Cas9 (Clontech 632607) at 1:150 dilution, anti-MAP2 (Millipore Ab5622) at 1:1000 dilution, SOX2 and PAX6. The cells were then stained with species specific secondary antibodies conjugated to Alexa 488, 568, or 635 fluorophores and mounted using Prolong Gold with DAPI. Images were captured on an inverted Olympus FV1000 laser-scanning confocal microscope.

ES Cell Line Derivation and Characterization

Human embryos were donated, under two conditions, to MStem Cell Laboratory's Institutional Review Board (IRB) approved study (HUM00028742) entitled "*Derivation of human Embryonic Stem Cells.*" Written informed consent was obtained for all embryo donations. First, embryos made for reproductive purposes, not genetically tested, frozen and no longer required for reproduction were donated (e.g., UM4-6). Second, partners with a known history of familial Fragile-X elected to perform *in vitro* fertilization and PGD, irrespective of embryo donation, to reduce the risk of having a child with Fragile X-spectrum disorder. The female partner was an *FMR1* pre-mutation carrier with a mutant allele determined to have 108 and 115 CGG repeats on two separate evaluations. The female partner had three paternal uncles with Fragile X-spectrum disorder. *In vitro* produced embryos were biopsied as blastocysts on day 5 of development, and trophectoderm cells were genetically assessed by an off-site genetic analysis company. Blastocysts were vitrified and cryo-stored until PGD results were obtained. Embryos with PGD results showing the mutant maternal haplotype and

no paternal X chromosome (affected male) where consented for donation and shipped to MStem Cell Laboratory (e.g., UM139-2).

Following hESC production and characterization, documents demonstrating adherence to NIH-established guidelines for embryo donation and hESC production of UM4-6 and UM139-2 were submitted to NIH for placement on the NIH hESC Registry and approvals were granted on 02/02/2012 (Registration # -0147) and 09/29/2014 (Registration # -0292), respectively. Derivation of hESCs and their derivatives prior to acceptance on the NIH registry were performed with non-federal funds. Additionally, studies after placement on the NIH registry were also supported by non-federal funds. Briefly, blastocyst morphology was assessed 4 h after embryos were warmed and dictated the mode of hESC derivation. Laser-dissected inner cell masses (ICMs) were plated on human foreskin fibroblast (HFF)—feeders to obtain early hESC colonies that were manually split after 5–7 days and expanded on HFF for establishment and characterization of hESC lines. hESC lines were tested for pluripotency marker expression (Oct4, Nanog, Sox2) by Q-PCR and protein expression by immunofluorescence (Oct4, Nanog, Sox2, SSEA4 and TRA-1-60). hESCs were differentiated for 21 days in culture as embryoid bodies and tested for expression of lineage markers by Q-PCR of endoderm (α-fetoprotein (AFP) and GATA4), mesoderm (brachyury and VE-Cadherin (VE-Cad)) and ectoderm (TUJ-1 and keratin-18 (Krt-18)). Finally, G-band karyotyping of UM4-6 and UM139-2 demonstrated euploid hESC lines.

Culture and Transfection of hESCs

Undifferentiated hESCs were cultured in mTeSR1 media (Stem Cell Technology) on Matrigel-coated plates with daily media changes and were passaged at 1:5–1:10 using L7 passaging media (Lonza) or 1 mM EDTA. For transfections, undifferentiated hESCs or NPCs derived by directed differentiation of hESCs were plated on Matrigel-coated plates in mTeSR1 media containing 10 μM Rock Inhibitor and grown overnight. Media was replaced with mTeSR1 the next day. Cells were allowed to recover for at least 4 h and media was replaced again just prior to transfections. Transfections were performed using plasmids as described above and TransIT LT1 transfection reagent (Mirus Bio) according to manufacturer's instructions. For NPC studies, transfections were done after a 14-day differentiation. Typical transfection efficiencies in hESCs and in NPCs were 40%–50% as measured by GFP fluorescence, and only samples with sufficient transfection rates were used in subsequent studies. Cells were cultured with daily media changes and harvested 48 h after transfection for RNA isolation and 72 h after transfection for western blots.

Southern Blot

Southern blotting was performed as in Gold et al. (2000) with modifications. Briefly, genomic DNA was isolated using the Qiagen DNeasy Blood and Tissue kit. 10 ug of genomic DNA from each cell line was digested with HindIII and EagI overnight. The digoxigenine (DIG)-labeled probe was amplified from the pE5.1 plasmid, using forward primer:

CGCCAAGAGGGCTTCAGGTCTCCT and reverse primer: GAGACTGTTAAGAACCTAAACGCGGG. The digested genomic DNA was resolved on a 0.7% agarose gel prior to Southern blotting. The nylon membrane was processed using the commercially available DIG Easy Hyb solution and DIG Wash and Block Buffer Set (Roche). DIG was antibody labeled with Anti-DIG-AP, Fab fragments (Sigma), processed using CDP-Star substrate (ThermoFisher) and detected on film. A wild-type band (~20 repeats) in Control lines appears at ~2.8 kb, whereas the expanded and methylated repeat in the Fragile X line appears at ~7.6 kb (800 + repeats) which is ~2.4 kb above where a non-expanded, methylated DNA fragment would appear (~5.2 kb).

Methylation qPCR

FMR1 methylation determination was made as previously described with minor modifications (de Esch et al., 2014). Briefly, genomic DNA was isolated from cell lines using the Qiagen DNeasy Blood and Tissue Kit. 2 ug of DNA from each was bisulfite converted using the EpiTect Bisulfite kit (Qiagen). qPCR was performed on 100 ng of bisulfite converted DNA using the iQ SYBR Green supermix (BioRad). The primers used were designed against the sense strand of *FMR1* and are previously described (de Esch et al., 2014). *FMR1* methylation-specific primers, forward: GGTCGAAAGATA GACGCGC and reverse: AAACAATGCGACCTATCACCG; *FMR1* unmethylated-specific primers, forward: TGTTGG TTTGTTGTTTGTTTAGA and reverse: AACATAATTTCA ATATTTACACCC; and primers for the housekeeping gene *CLK2*, which is constitutively active in stem cells and should therefore not undergo CpG methylation in the region of amplification, forward: CGGTTGATTTTGGGTGAAGT and reverse: TCCCGACTAAAATCCCACAA. Methylation-specific and unmethylated-specific qPCR analyzed neighboring but non-overlapping regions with 11 and 15 methylation sites, respectively. The efficiency of the primers was between 95% and 100%. Amplification of both methylated and unmethylated *FMR1* was normalized to *CLK2*, then a ratio was created using the two values. In control fibroblasts where no amplification was detected with the methylation-specific primers, methylation was set at 0%.

Directed Differentiation of hESC to NPCs and Neurons

Neural induction was performed using a dual-SMAD inhibition (Shi et al., 2012) protocol with modifications. In brief, undifferentiated hESCs in two wells of a 6-well plate were grown to approximately 80% confluence, dissociated with EDTA, and plated into a single well of a Matrigel-coated 6-well plate with TeSR-E8 containing 10 µM Rock Inhibitor (Y-27632). The cells were confluent the next day and neural differentiation was induced using neural maintenance media (referred to here as 3N) containing 1 µM dorsomorphin and 10 µM SB431542. The cells were cultured for 12–14 days with daily media changes. Neuroepithelial sheets were then combed into large clumps, passaged and maintained on Matrigel-coated plates in rosette media (3N containing 20 ng/ml FGF2) with

daily media changes until neural rosettes appeared. Rosettes were manually picked and dissociated into single cells using Accutase. NPCs were plated onto Matrigel-coated plates, grown in neural expansion media (3N containing 20 ng/ml FGF and 20 ng/ml EGF) with media changes every other day, and passaged as needed using Accutase. For differentiation into neurons, NPCs were plated at a density of approximately 1.5×10^5 cells/mL in neural expansion media on PLO-laminin coated plates or coverslips, allowed to grow for 24 h, and switched to neural maintenance media. Neurons were maintained for up to 6 weeks with half media changes every other day and a full media change supplemented with 1 µg/ml laminin every 10 days.
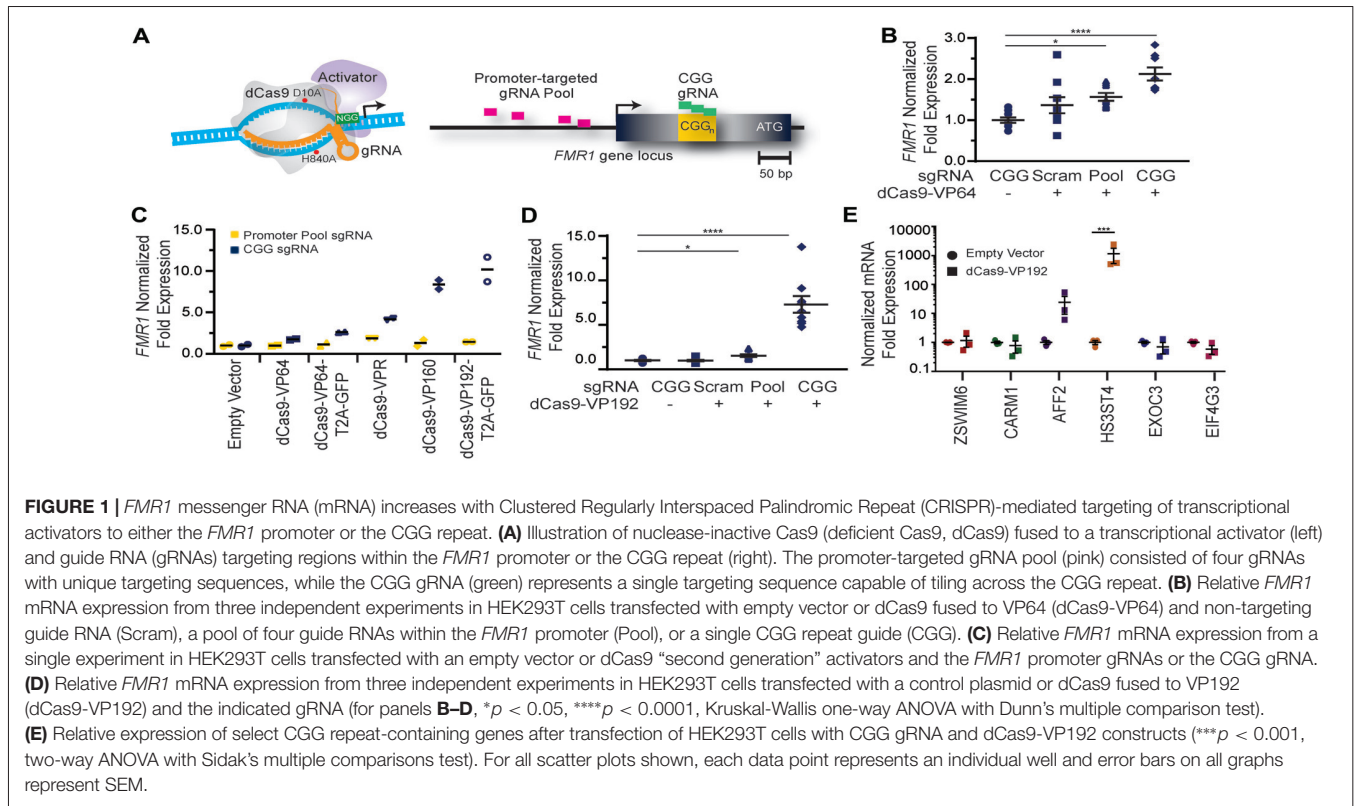
RNA Sequencing and GO Analysis

Sequencing was performed by the UM DNA Sequencing Core, using the Illumina Hi-Seq 4000 platform, single end, 50 cycles, mRNA prep. At the UM Bioinformatics Core, files from the Sequencing Core's storage were concatenated into a single fastq file for each sample. The quality of the raw reads data for each sample was checked using FastQC[1] (version 0.11.3) to identify features of the data that may indicate quality problems (e.g., low-quality scores, over-represented sequences, inappropriate GC content). The Tuxedo Suite software package was used for alignment, differential expression analysis and post-analysis diagnostics (Langmead et al., 2009; Trapnell et al., 2009, 2013). Briefly, the reads were aligned to the reference mRNA transcriptome (hg19[2]) using TopHat (version 2.0.13) and Bowtie2 (version 2.2.1.). Default parameter settings for alignment were used, with the exception of: "—b2-very-sensitive" telling the software to spend extra time searching for valid alignments. FastQC was used for a second round of quality control (post-alignment), to ensure that only high-quality data would be input to expression quantitation and differential expression analysis. Cufflinks/CuffDiff (version 2.2.1) was used for expression quantitation, normalization and differential expression analysis, using hg19.fa as the reference genome sequence. For this analysis, the parameter settings were: "—multi-read-correct" to adjust expression calculations for reads that map in more than one locus, as well as "—compatible-hits-norm" and "—upper-quartile–norm" for normalization of expression values. Diagnostic plots were generated using the CummeRbund R package. Locally developed scripts were used to format and annotate the differential expression data output from CuffDiff. Briefly, genes and transcripts were identified as being differentially (DE) expressed based on three criteria: test status = "OK", FDR ≤ 0.05, and fold change $\geq \pm 1.5$. Genes and isoforms were annotated with NCBI Entrez GeneIDs and text descriptions. iPathwayGuide (Advaita Corporation[3]) was used to model the biological relevance of DE genes for each algorithm, as well as a meta-analysis comparing the two approaches.

---

[1]https://www.bioinformatics.babraham.ac.uk/projects/fastqc/
[2]http://genome.ucsc.edu/
[3]http://www.advaitabio.com

FIGURE 1 | *FMR1* messenger RNA (mRNA) increases with Clustered Regularly Interspaced Palindromic Repeat (CRISPR)-mediated targeting of transcriptional activators to either the *FMR1* promoter or the CGG repeat. **(A)** Illustration of nuclease-inactive Cas9 (deficient Cas9, dCas9) fused to a transcriptional activator (left) and guide RNA (gRNAs) targeting regions within the *FMR1* promoter or the CGG repeat (right). The promoter-targeted gRNA pool (pink) consisted of four gRNAs with unique targeting sequences, while the CGG gRNA (green) represents a single targeting sequence capable of tiling across the CGG repeat. **(B)** Relative *FMR1* mRNA expression from three independent experiments in HEK293T cells transfected with empty vector or dCas9 fused to VP64 (dCas9-VP64) and non-targeting guide RNA (Scram), a pool of four guide RNAs within the *FMR1* promoter (Pool), or a single CGG repeat guide (CGG). **(C)** Relative *FMR1* mRNA expression from a single experiment in HEK293T cells transfected with an empty vector or dCas9 "second generation" activators and the *FMR1* promoter gRNAs or the CGG gRNA. **(D)** Relative *FMR1* mRNA expression from three independent experiments in HEK293T cells transfected with a control plasmid or dCas9 fused to VP192 (dCas9-VP192) and the indicated gRNA (for panels **B–D**, *p < 0.05, ****p < 0.0001, Kruskal-Wallis one-way ANOVA with Dunn's multiple comparison test). **(E)** Relative expression of select CGG repeat-containing genes after transfection of HEK293T cells with CGG gRNA and dCas9-VP192 constructs (***p < 0.001, two-way ANOVA with Sidak's multiple comparisons test). For all scatter plots shown, each data point represents an individual well and error bars on all graphs represent SEM.

RESULTS

Transcriptional Activation of the *FMR1* Gene by CRISPR-dCas9 Fused to VP16 Activation Domains

To determine whether use of CRISPR targeted transcriptional activators could augment *FMR1* expression, we first tested them in HEK 293T cells that have a normal sized (23) CGG repeat in the 5′UTR of the *FMR1* gene. We designed multiple guide RNAs (gRNAs) to the promoter region or to the CGG repeat of the *FMR1* gene. These gRNAs were used along with the catalytically-inactive dCas9 fused to different versions of the VP16 transcriptional activation domain (**Figure 1A**). At 48 h post transfection, we observed a significant increase in *FMR1* transcript levels using the dCas9-VP64 construct with both the promoter pool and CGG gRNAs (**Figure 1B**) compared to a scrambled control gRNA or to cells transfected with only GFP. We next compared activation efficiencies for both sets of gRNAs with different versions of dCas9 fused with either the chimeric activation domain VPR (composed of the activation domains of VP64, p65 and Rta linked in tandem), or multiple domains of VP16 (**Figure 1C**). The strongest transcriptional activation in heterologous cells was achieved with a CGG repeat-targeted dCas9-VP192, which yielded approximately an 8-fold increase in *FMR1* mRNA levels (**Figures 1C,D**). The CGG repeat targeted guide robustly increased *FMR1* transcript levels compared to the promoter-pool gRNAs, suggesting that its repetitive binding sites augment the targeting strategy (**Figure 1D**).

Because CGG tandem microsatellites are not unique within the genome, we also queried six candidate genes with CGG repeats in their 5′UTR for off target effects in HEK293T cells. We observed an increase in transcript levels for the *AFF2* gene (also called *FXR2*) and *HS3ST4* gene suggesting potential off-target effects in this cell type with a repeat-targeting strategy (**Figure 1E**). However, the effects on *AFF2* are potentially interesting clinically. Expansion of this CCG repeat triggers hypermethylation and transcriptional silencing of the *AFF2* gene, in a fashion that is quite similar to FXS (also known as FRAXA). This results in FRAXE, a rare genetic form of autism and intellectual disability (Knight et al., 1993; Gecz et al., 1996). Together, these data demonstrate that the dCas9-VP192 system can effectively activate transcription of the *FMR1* gene. Additionally, CGG gRNA provide more robust activation compared to promoter pool gRNAs but with a greater potential for off-target effects.

dCas9-VP192 Increases FMRP Levels in HEK293T Cells

We next determined if the observed transcriptional changes correlated with enhanced production of FMRP. FMRP levels were measured in HEK293T cells transfected with either the promoter pool or CGG-repeat targeted gRNAs and the dCas9-VP192 construct. By immunocytochemistry, cells transfected with CRISPR constructs show an increase in FMRP signal with either CGG or promoter targeted gRNAs, but not with scramble guide RNA (**Figure 2A**). Western blot analysis of transfected cells demonstrated a significant increase in FMRP protein in
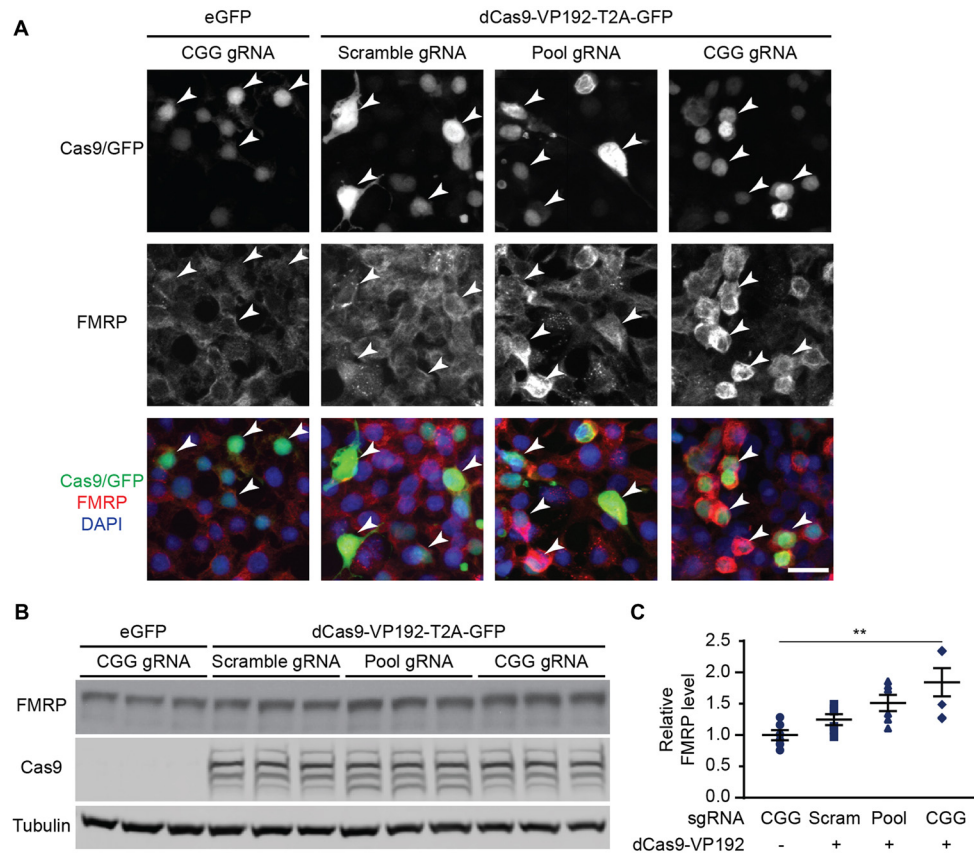
FIGURE 2 | CRISPR-mediated transcriptional activation increases FMRP protein abundance at normal CGG repeat sizes. **(A)** Immunocytochemistry of HEK293T cells transfected with eGFP or dCas9-VP192 and gRNAs, as indicated. Single channel and merged images are shown with Cas9/GFP (green), FMRP (red), and DAPI (blue). White arrowheads indicate transfected cells. Scale bar represents 20 μm. **(B)** Western blots showing triplicate samples of HEK293T cells transfected with control plasmid (eGFP) or with dCas9-VP192 and indicated gRNAs and immunoblotted for FMRP, Cas9 and Tubulin. **(C)** Quantification of western blots from HEK293T cells transfected as indicated. Data are shown as FMRP normalized to tubulin and relative to the control plasmid ($n = 6$/group evaluated over at least two independent experiments). **$p < 0.01$, Kruskal-Wallis one-way ANOVA with Dunn's multiple comparison test). Error bars represent SEM.

CGG repeat targeted gRNAs compared to control transfections (**Figures 2B,C**). Thus, targeted activation of the *FMR1* gene using a dCas9-VP192 system increases both *FMR1* mRNA and FMRP levels in human cells at normal repeat sizes.
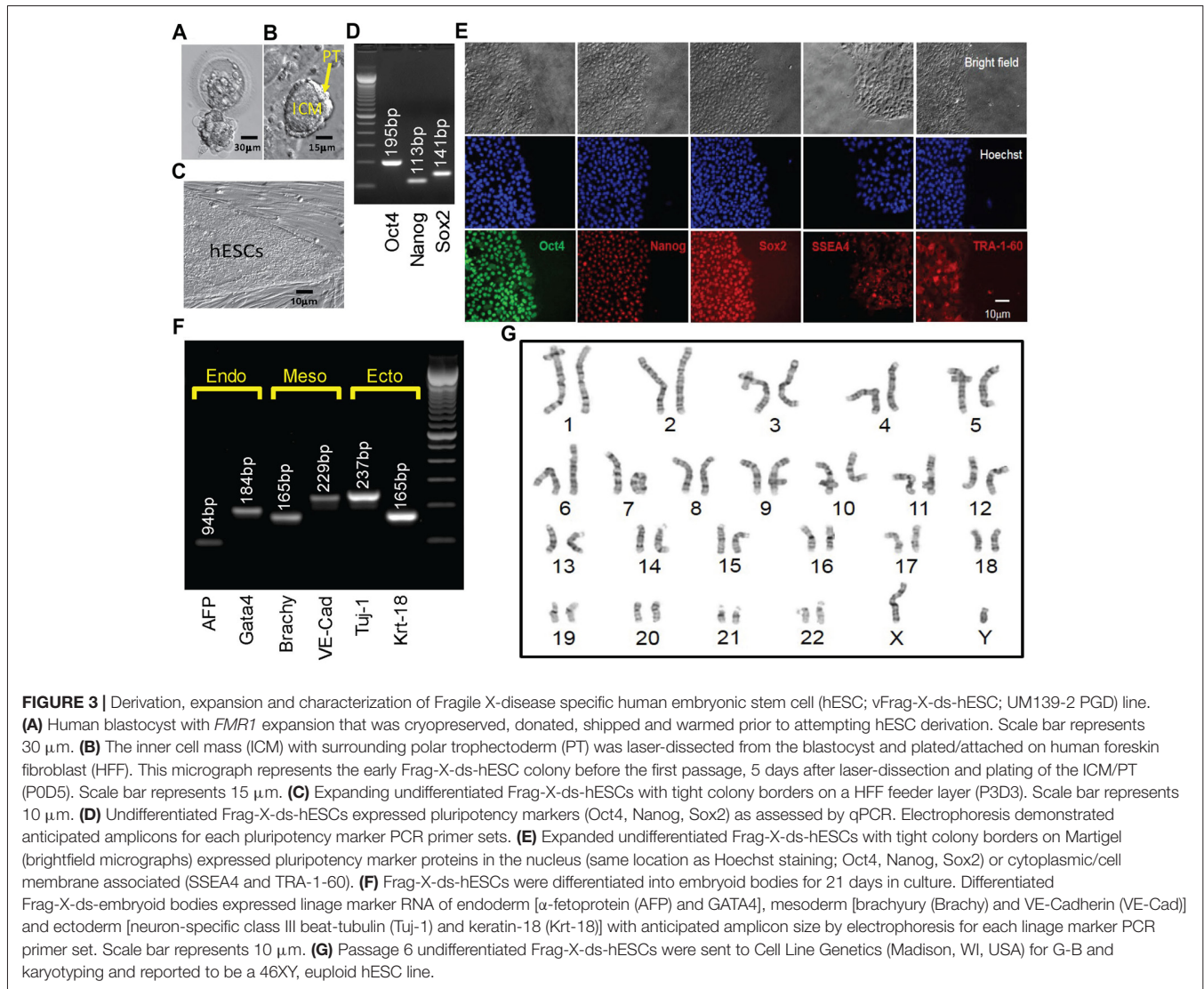
FXS hESCs Exhibit Passage-Dependent Silencing of *FMR1* Prior to Neuronal Differentiation

An important first step in developing a method for reactivation of *FMR1* transcription is identifying a model that recapitulates the developmental epigenetic silencing that occurs in FXS patients. Until recently, the UM139-2 PGD hESC line was the only Fragile X hESC line on the NIH registry of approved lines for federally-funded research in the United States[4]. However, different Fragile X hESC lines exhibit variability in terms of their methylation and *FMR1* transcription (Avitzour et al., 2014). We therefore characterized this new FXS hESC line.

---

[4]https://stemcells.nih.gov/research/registry.htm

The embryo from which this hESC line (UM 139-2) was derived was determined to be affected with FXS through PGD. This blastocyst was cryopreserved after testing and sent to MStem Cell laboratories, where derivation of hESCs took place (**Figures 3A–C**). Pluripotency and fidelity of this line was confirmed by RT-PCR and immunohistochemistry for pluripotency markers (**Figures 3D,E**). The line was capable of embryoid body formation containing all three germ layers, consistent with pluripotency (**Figure 3F**). DNA fingerprinting and karyotyping demonstrated a 46XY euploid genetic background (**Figure 3G**).

We next characterized the line in terms of its Fragile X mutation. Southern blot analysis indicated that this hESC line contains a Fragile X full mutation with approximately 800 CGG repeats (**Figure 4A**). The first characterized FXS hESC line, HE-FX, exhibited no methylation in the hESC state, but instead demonstrated methylation and transcriptional silencing with cellular differentiation (Eiges et al., 2007). However, more recent studies suggest that this property is not universal, with some Fragile X hESCs exhibiting early

FIGURE 3 | Derivation, expansion and characterization of Fragile X-disease specific human embryonic stem cell (hESC; vFrag-X-ds-hESC; UM139-2 PGD) line. **(A)** Human blastocyst with *FMR1* expansion that was cryopreserved, donated, shipped and warmed prior to attempting hESC derivation. Scale bar represents 30 μm. **(B)** The inner cell mass (ICM) with surrounding polar trophectoderm (PT) was laser-dissected from the blastocyst and plated/attached on human foreskin fibroblast (HFF). This micrograph represents the early Frag-X-ds-hESC colony before the first passage, 5 days after laser-dissection and plating of the ICM/PT (P0D5). Scale bar represents 15 μm. **(C)** Expanding undifferentiated Frag-X-ds-hESCs with tight colony borders on a HFF feeder layer (P3D3). Scale bar represents 10 μm. **(D)** Undifferentiated Frag-X-ds-hESCs expressed pluripotency markers (Oct4, Nanog, Sox2) as assessed by qPCR. Electrophoresis demonstrated anticipated amplicons for each pluripotency marker PCR primer sets. **(E)** Expanded undifferentiated Frag-X-ds-hESCs with tight colony borders on Martigel (brightfield micrographs) expressed pluripotency marker proteins in the nucleus (same location as Hoechst staining; Oct4, Nanog, Sox2) or cytoplasmic/cell membrane associated (SSEA4 and TRA-1-60). **(F)** Frag-X-ds-hESCs were differentiated into embryoid bodies for 21 days in culture. Differentiated Frag-X-ds-embryoid bodies expressed linage marker RNA of endoderm [α-fetoprotein (AFP) and GATA4], mesoderm [brachyury (Brachy) and VE-Cadherin (VE-Cad)] and ectoderm [neuron-specific class III beat-tubulin (Tuj-1) and keratin-18 (Krt-18)] with anticipated amplicon size by electrophoresis for each linage marker PCR primer set. Scale bar represents 10 μm. **(G)** Passage 6 undifferentiated Frag-X-ds-hESCs were sent to Cell Line Genetics (Madison, WI, USA) for G-B and karyotyping and reported to be a 46XY, euploid hESC line.

methylation and silencing. To evaluate whether the repeat was methylated in UM 139-2 hESC line, we performed methylation-specific quantitative-PCR on early passage (<20 passages) and late passage (>30 passages) FXS hESCs. This demonstrated a passage-dependent methylation of the *FMR1* promoter region with earlier passages displaying incomplete methylation and later passages displaying complete methylation as compared to control hESCs and FXS fibroblasts, respectively (**Figure 4B**).

To determine the impact of this methylation on *FMR1* transcriptional activity, we measured *FMR1* mRNA expression by qRT-PCR. This demonstrated a passage-dependent shift in expression in FXS hESCs. At early passages, *FMR1* mRNA levels were only modestly decreased (30%) compared to controls. However, after continued passages (typically >30 passages, with some variability), *FMR1* mRNA levels became nearly undetectable (0.4% of control levels, **Figure 4C**). We observed a similar passage-dependent change in FMRP protein level,

although there was a significant deficit in FMRP expression even at early passage numbers, perhaps due to translational blockade (**Figure 4D**; Feng et al., 1995; Chen et al., 2003; Iliff et al., 2013).

To confirm that the absence of FMRP does not preclude differentiation into neurons from FXS hESCs, we performed directed neuronal differentiation using a dual SMAD inhibitor-based differentiation protocol (Shi et al., 2012). This method successfully produced hESC-derived PAX-6 and MAP2 positive neural rosettes and FXS neurons (**Figures 4E–G**). As reported previously for other FXS lines, we also observed a slight delay in neural rosette formation as well as a lower density of neurons from the UM 139-2 FXS line (Telias et al., 2013). Combined, these data suggest that UM 139-2 FXS hESCs are a good model for investigating methods of reactivating *FMR1* transcription, and the feature of time-dependent transcriptional silencing allows for targeting of reactivation at expanded repeats in different epigenetic contexts.
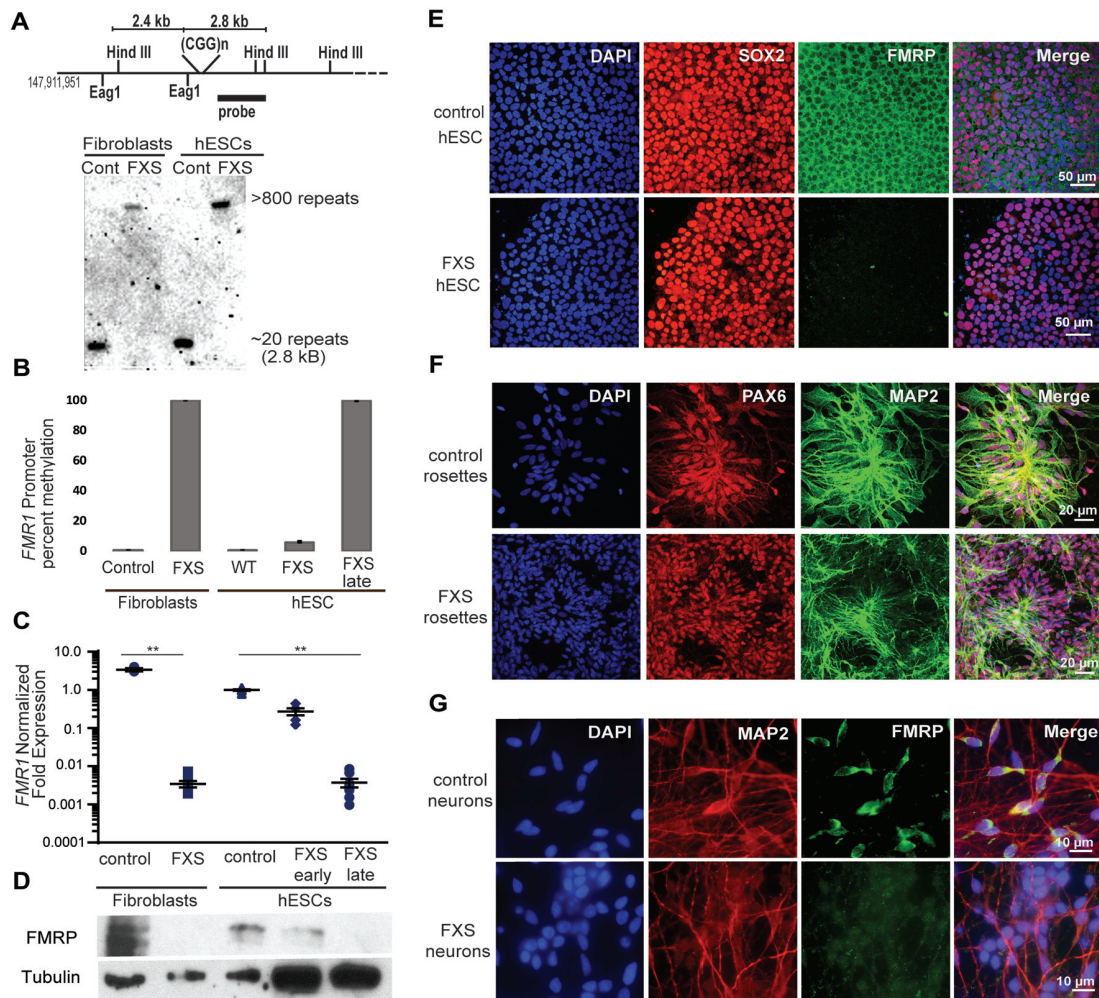
FIGURE 4 | Fragile X hESC line (UM139-2 PGD) carries a large CGG repeat and undergoes passage dependent transcriptional silencing. **(A)** Top panel: schematic representing the *Eag1* and *Hind III* restriction sites on the *FMR1* genomic locus, the digoxigenine (DIG)-labeled probe used for Southern blotting in this study and the expected fragment sizes. The figure is not to scale. Bottom panel- Southern blot shows CGG repeat length and methylation status for genomic DNA from control and Fragile X Syndrome (FXS) patient-derived fibroblasts and hESCs. Repeat size is estimated at <800. **(B)** Bisulfite-qPCR using methylation-specific primers reveals a passage dependent methylation at the *FMR1* promoter for genomic DNA from indicated cells. Data shown for two independent experiments. **(C)** Relative *FMR1* transcript levels in control and FXS patient-derived fibroblasts and hESCs. FXS hESCs were assessed at early passages (P13–20) and late passages (P30+). **p < 0.01, Kruskal-Wallis one-way ANOVA with Dunn's multiple comparison test, data from five independent experiments, error bar represents SEM. **(D)** Western blots showing FMRP and tubulin in control and FXS patient-derived fibroblasts as well as control hESC and early and late passage FXS hESCs. One-tenth of the lysate was loaded for control fibroblasts and control hESCs. **(E)** Undifferentiated control and FXS hESC colonies immunostained for FMRP (green), pluripotency marker SOX2 (red) and DAPI (blue). Scale bars represent 50 μm. **(F)** Neural rosettes derived from control and FXS hESCs with neuronal lineage marker MAP2 (green), neuroectoderm maker PAX6 (red), and DAPI (blue) immunostaining. Scale bars represent 20 μm. **(G)** Neurons derived from control and FXS hESCs shown with FMRP (green), MAP2 (red) and DAPI (blue) immunostaining. Scale bars represent 10 μm.

dCas9-VP192 Activates *FMR1* Transcription in FXS hESCs and NPCs

Based on our success using dCas9-VP192 to activate transcription of the *FMR1* gene in HEK293T cells, we first tested the same constructs and gRNAs in control hESCs. Control hESCs showed a significant increase in *FMR1* transcript levels using the promoter targeted gRNAs with dCas9-VP192 only (**Figure 5A**), although the effects were more variable and less robust than those observed in HEK293T cells. We next evaluated whether this increase in mRNA was associated with

changes in protein expression. By immunohistochemistry, there was a clear relationship between cells expressing the dCas9 construct and an increase in FMRP expression for the promoter pool gRNAs but not the CGG repeat gRNAs (**Figure 5B**). By western blot as well, only the promoter pool targeted gRNAs demonstrated a significant change in protein expression (**Figures 5C,D**). This discrepancy may reflect differences in efficiency of translation and expression from these vectors between HEK293T cells and hESCs.
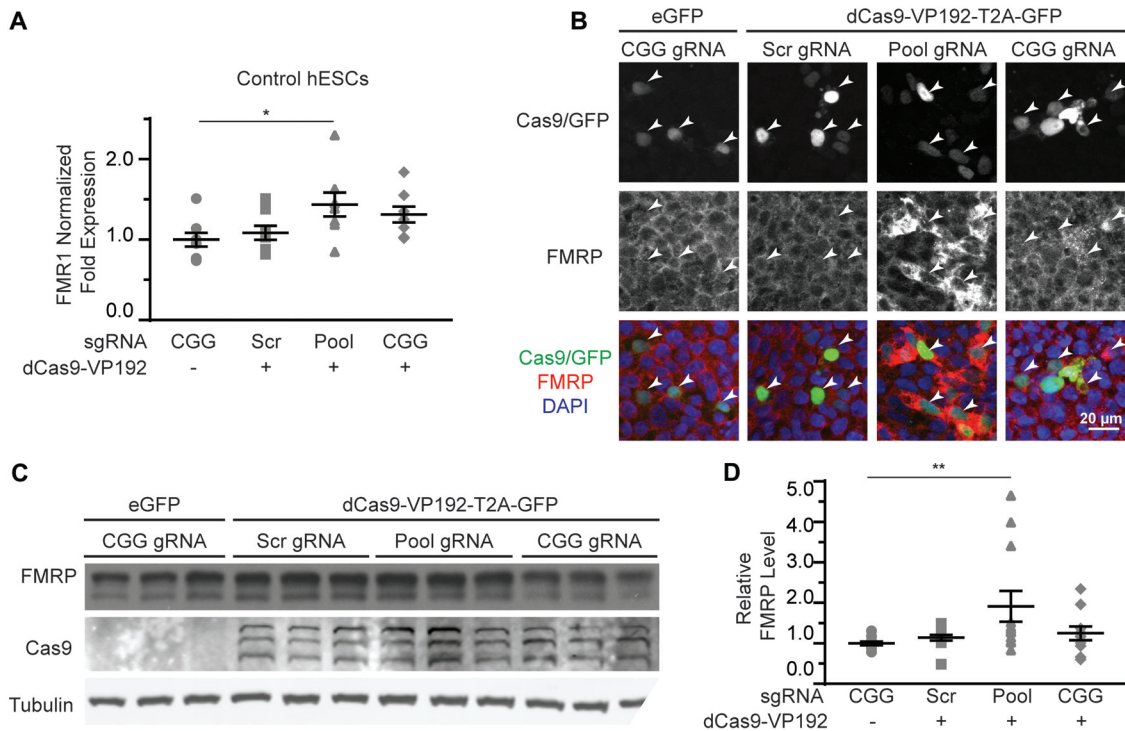
FIGURE 5 | CRISPR-mediated activation enhances *FMR1* transcription and FMRP protein abundance in control hESCs. **(A)** Relative *FMR1* mRNA expression in control (UM4-6) hESCs transfected with a control plasmid or dCas9-VP192 and the indicated gRNAs (*$p < 0.05$, Kruskal-Wallis one-way ANOVA with Dunn's multiple comparison test). **(B)** Images of control hESCs transfected with eGFP or dCas9-VP192 and gRNAs, as indicated. Single channel and merged images are shown with Cas9/GFP (green), FMRP (red) and DAPI (blue). Arrowheads indicate transfected cells. Scale bar represent 20 μm. **(C)** Western blots showing triplicate samples of control hESCs transfected and immunoblotted as indicated. **(D)** Quantification of western blots from control hESCs transfected as indicated. Data are shown as FMRP levels normalized to tubulin and relative to the control plasmid (**indicates $p = 0.0061$ by Kruskal-Wallis one-way ANOVA with Dunn's multiple comparison test). For all scatter plots, each data point represents an individual well. Data were obtained from three **(A)** or four **(D)** independent experiments. The mean with error bars (SEM) is shown for each condition.

We next tested whether the dCas9-VP192 system could re-activate or enhance transcription from the *FMR1* locus in UM139-2 FXS hESCs. Because of their baseline differences in *FMR1* transcription, we evaluated both early and late passage hESCs. In early passage FXS hESCs, both the promoter and CGG gRNAs elicited a 1.3-fold and a 1.8-fold increase, respectively in *FMR1* transcript levels compared to the scrambled guide RNA in the same line (**Figure 6A**). However, this increase was significantly greater with the CGG guide RNAs compared to the promoter targeting gRNAs (**Figure 6A**).

In late passage FXS hESCs *FMR1* mRNA levels were very low basally (**Figure 4C**). Treatment with scrambled gRNA or promoter targeted gRNAs in the setting of dCas9-VP192 had no impact on *FMR1* RNA expression. However, CGG targeted gRNA coupled with dCas9-VP192 led to a marked increase in *FMR1* mRNA expression-upwards of 20-fold in some samples (**Figure 6B**). Thus, at both a partially and completely transcriptionally silenced CGG full mutation locus, we observed that targeting a transcriptional activator directly to the repeats elicited the greatest enhancement of *FMR1* mRNA expression. Next, we differentiated the control and late FXS hESCs to NPCs and tested for *FMR1* transcript levels after treating them with

the dCas9-VP192 and gRNAs. The NPCs differentiated from the late FXS hESCs were selected since they did not have any baseline *FMR1* transcription, which reflected the disease state more closely. Similar to our observations in undifferentiated hESCs, control NPCs showed a statistically significant increase in *FMR1* levels using the promoter pool targeted gRNAs (**Figure 6C**) while the FXS NPCs showed the same increase in transcript level with the CGG gRNA only (**Figure 6D**). Thus, the effects of specific gRNAs with dCas9-VP192 on *FMR1* mRNA expression are different in the setting of large CGG repeat expansions, but consistent across cell differentiation states.

CGG Repeat Targeted gRNA Shows Minimal Off Target Effects in FXS hESCs

We next evaluated whether there were off-target effects elicited by the CGG repeat targeted gRNAs. We first queried the six candidate genes identified in HEK293T cells (**Figure 1E**). Unlike the case in HEK293T cells, we saw no increase in their mRNA levels in FXS hESCs expressing CGG gRNA and dCas9-VP192 (**Figure 7A**). To evaluate genome-wide off-target effects elicited by expression of CGG gRNA and dCas9-VP192, we performed
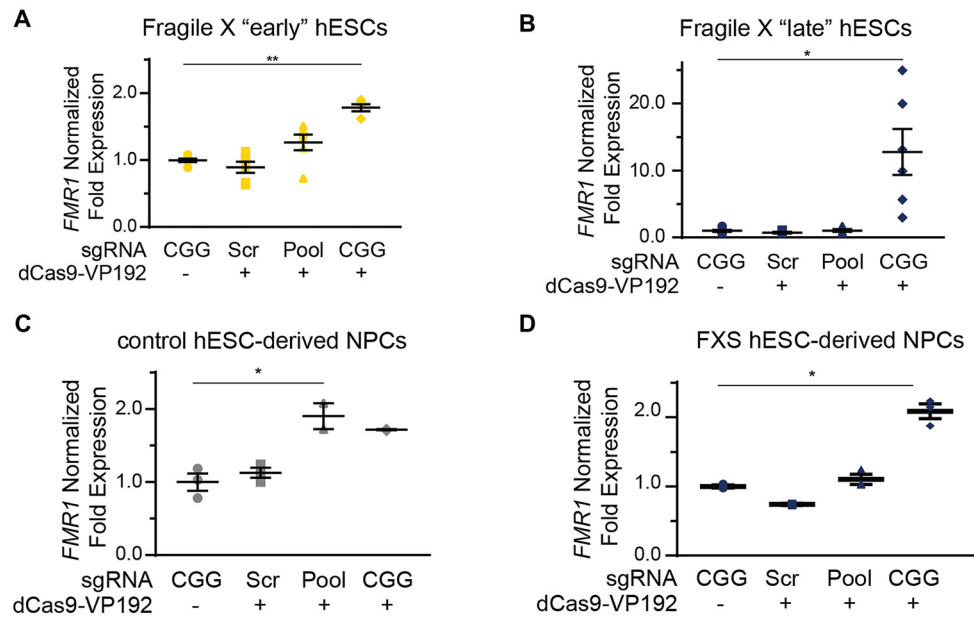
FIGURE 6 | Targeting CRISPR-dCas9-VP192 to the CGG repeat overcomes transcriptional silencing and selectively enhances transcription of *FMR1* in FXS hESCs and neural progenitor cells (NPCs). **(A)** Relative *FMR1* mRNA expression in early (P23–25) passage FXS hESCs transfected with control plasmid or dCas9-VP192 and the indicated gRNA (**$p < 0.01$, *$p < 0.05$, Kruskal-Wallis one-way ANOVA with Dunn's multiple comparison test). **(B)** Relative *FMR1* mRNA expression in late (P53–57) passage FXS hESCs transfected with control plasmid or dCas9-VP192 and the indicated gRNA (**$p < 0.01$, *$p < 0.05$, Kruskal-Wallis one-way ANOVA with Dunn's multiple comparison test). **(C)** Relative *FMR1* mRNA expression in control hESC-derived NPCs at 48 h after transfection with control plasmid or dCas9-VP192 after differentiation with the indicated gRNAs (*$p < 0.05$, Kruskal-Wallis one-way ANOVA with Dunn's multiple comparison test). **(D)** Relative *FMR1* mRNA expression in late FXS hESC-derived NPCs transfected with control plasmid or dCas9-VP192 with the indicated gRNAs (*$p < 0.05$, Kruskal-Wallis one-way ANOVA with Dunn's multiple comparison test). For all scatter plots, each data point represents an individual well. Data were obtained from two independent experiments. The mean with error bars (SEM) is shown for each condition.

RNA-seq analysis of FXS hESCs treated with scramble gRNA vs. CGG gRNA and dCas9-VP192 (**Figures 7B,C**). A comparison between FXS hESCs treated with scrambled or CGG gRNA and dCas9-VP192 showed only 35 genes out of 23,394 that were differentially expressed (DE) between these two conditions (**Figure 7C**).
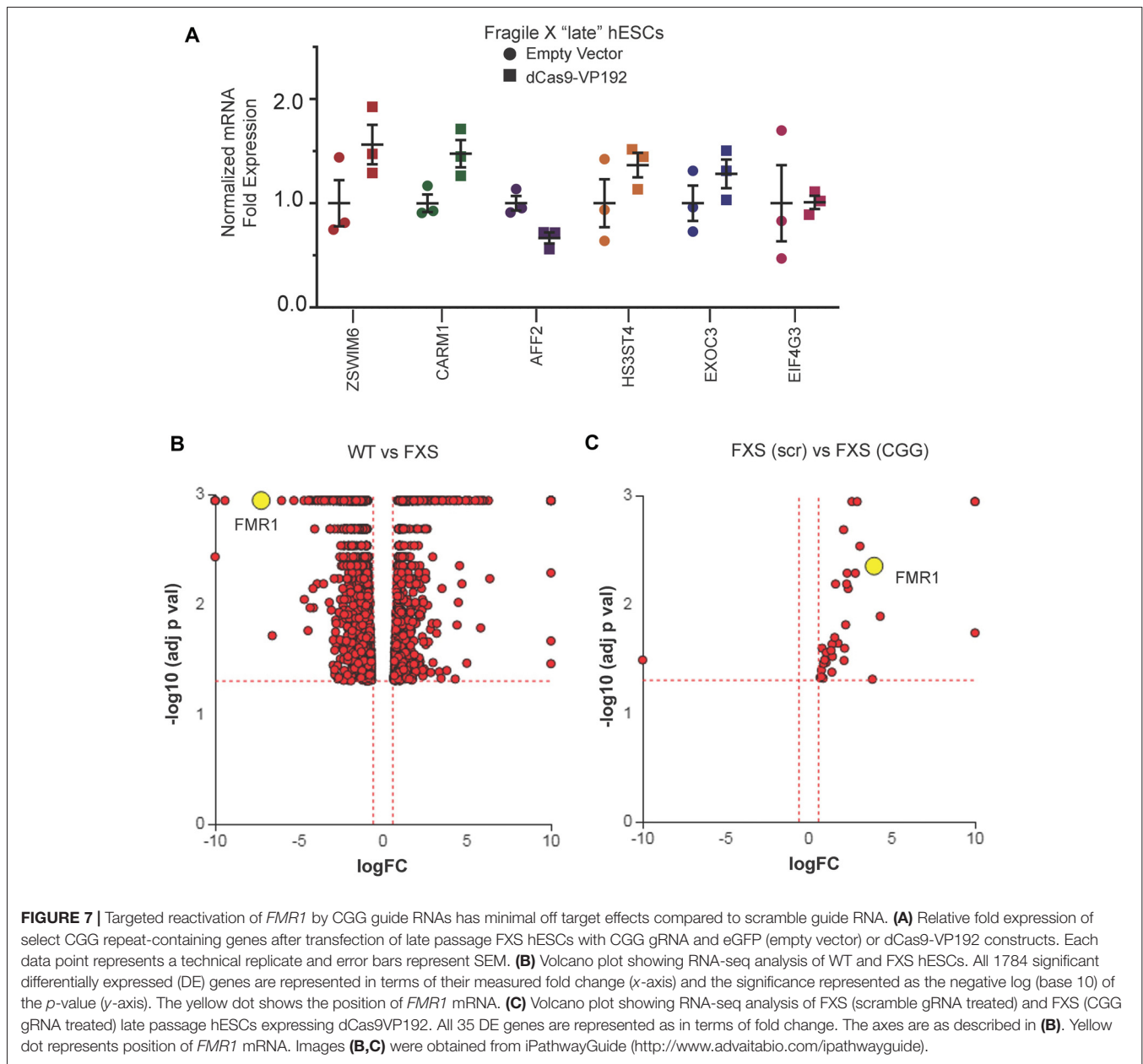
In parallel, we also performed RNA-seq to identify if there were any significant transcriptional differences between our FXS hESC line and our control hESC line (**Figure 7B**). A total of 1,797 genes were found to be DE between untreated WT and FXS hESCs. As expected, *FMR1* expression was much lower in the FXS hESCs. Gene Ontology analysis comparing the WT and FXS hESCs datasets identified nervous system development and neurogenesis as particularly different between these two hESC lines (**Supplementary Figure S1A**). Additionally, DE genes between these two hESC lines significantly map to cancer pathways (**Supplementary Figure S1B**). This data is consistent with studies suggesting that FMRP regulates mRNAs involved in cancer progression and metastasis (Lucá et al., 2013; Zalfa et al., 2017). However, one must be cautious in interpreting these differences in expression as resulting from the *FMR1* repeat expansion or loss of FMRP as these two hESC lines are not isogenic. Of note, treatment with CGG gRNA and dCas9-VP192 did not significantly revert FXS hESCs back towards the WT hESC transcriptomic profile (data not shown).

dCas9-VP192 Activation Does Not Increase FMRP Levels in FXS hESC

In order to test whether the increase in *FMR1* transcript levels would cause a subsequent increase in FMRP, we tested the early and late FXS hESC lines with the promoter pool and CGG targeted gRNAs along with dCasVP-192. Despite a significant increase in mRNA, we did not observe a statistically significant increase in FMRP levels in either early or late passage FXS hESCs (**Figures 8A–D**). Similar results were obtained with ICC measurements in these cells (data not shown). Thus, there is a dissociation at least in these cells between transcriptional reactivation and recovery of FMRP expression.

DISCUSSION

FXS results primarily from transcriptional silencing of the *FMR1* locus. Here, we report reactivation of *FMR1* transcription utilizing a CRISPR-dCas9 coupled transcriptional activator selectively targeted to the expanded CGG repeat. Enhanced transcription occurs at very large CGG repeat expansions in hESCs in the setting of incomplete and complete transcriptional silencing and despite DNA methylation of the locus. This transcriptional reactivation is also greatest when we use a guide RNA that directly targets the CGG repeat, and this effect is enhanced in the setting of a large CGG repeat expansion.

FIGURE 7 | Targeted reactivation of *FMR1* by CGG guide RNAs has minimal off target effects compared to scramble guide RNA. **(A)** Relative fold expression of select CGG repeat-containing genes after transfection of late passage FXS hESCs with CGG gRNA and eGFP (empty vector) or dCas9-VP192 constructs. Each data point represents a technical replicate and error bars represent SEM. **(B)** Volcano plot showing RNA-seq analysis of WT and FXS hESCs. All 1784 significant differentially expressed (DE) genes are represented in terms of their measured fold change (*x*-axis) and the significance represented as the negative log (base 10) of the *p*-value (*y*-axis). The yellow dot shows the position of *FMR1* mRNA. **(C)** Volcano plot showing RNA-seq analysis of FXS (scramble gRNA treated) and FXS (CGG gRNA treated) late passage hESCs expressing dCas9VP192. All 35 DE genes are represented as in terms of fold change. The axes are as described in **(B)**. Yellow dot represents position of *FMR1* mRNA. Images **(B,C)** were obtained from iPathwayGuide (http://www.advaitabio.com/ipathwayguide).

Unfortunately, while transcriptional activation correlated with an increase in FMRP expression in human cell lines with normal repeat sizes, we did not observe a significant increase in FMRP expression in FXS hESC cells. These findings provide proof-of-concept for a CRISPR based approach to gene reactivation in FXS patient cells with the potential for translation to *in vivo* systems, but with the caveat that large transcribed CGG repeats may introduce an additional blockade on FMRP translation.

Our approach uses a nuclease deficient Cas9 to target the CGG repeats for the reactivation of the *FMR1* gene. The use of a nuclease-deficient Cas9 fused to transcriptional activators or suppressors is a powerful tool for studying genome-scale events as well as specific processes (Wang et al., 2016). Similar transcriptional activator systems have been used previously

to successfully reverse disease symptoms in mouse models of Duchenne Muscular Dystrophy, highlighting the potential applicability of this system for *in vivo* treatment of disease (Long et al., 2016; Nelson et al., 2016). In our hands, dCas9-VP16 fusion constructs show the highest activation with a VP192 fusion construct along with the CGG repeated targeted gRNA. The robust activation observed using the CGG gRNA vs. a promoter-targeted construct is particularly intriguing, as it suggests that the repetitive nature of the CGG guide may serve to augment its targeting strategy by providing a promoter-proximal tiling site for dCas9-VP192 complexes. This is consistent with findings obtained from other groups targeting repeats as a method of transcriptional silencing of the locus (Pinto et al., 2017). It thus appears that repeat expansions
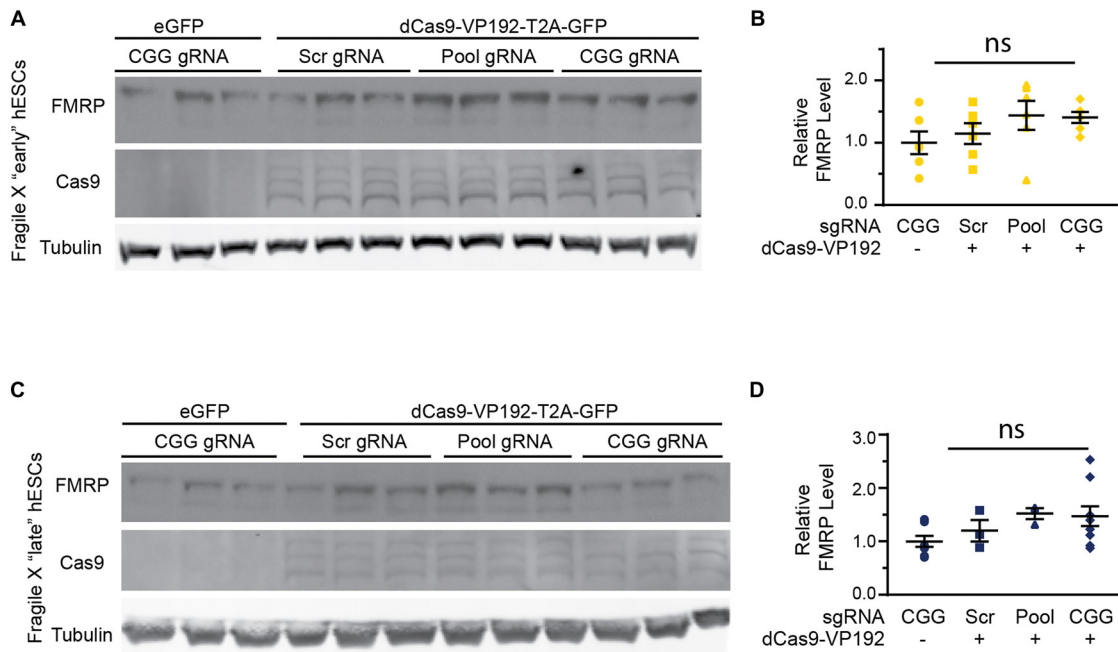
FIGURE 8 | Targeted reactivation of *FMR1* does not significantly enhance FMRP expression in FXS hESCs. **(A)** Western blots showing triplicate samples of early (P25–28) passage FXS hESCs transfected with control plasmid (eGFP) or with dCas9-VP192 and gRNAs immunoblotted for FMRP (by Femto ECL), Cas9 and tubulin as a loading control. **(B)** Quantification of western blots from early passage FXS hESCs transfected as indicated. **(C)** Western blots showing triplicate examples of late (P47–64) passage FXS hESCs transfected as in **(A)**. **(D)** Quantification of western blots from late passage FXS hESCs transfected as indicated. For all scatter plots, each data point represents an individual well. Data were obtained from two **(B)** or three **(D)** independent experiments. The mean with error bars (SEM) is shown for each condition. ns, not significant.

can recruit multiple dCas9-VP192 complexes simultaneously, with greater recruitment and potentially greater effect at larger repeat sizes. Additionally, evaluation of potential off-targets for this gRNA suggests that the presence of a large repeat element in FXS hESCs may suppress effects at other CGG repeat sites throughout the genome. Alternatively, there may be differences between hESCs and HEK293T cells in their basal transcriptomes that make them differentially sensitive to CGG repeat targeted gRNAs. This approach of directly targeting the repeats leverages the very nature of the repeat to achieve greater efficacy and specificity and has recently been used in other repeat expansion disorders to great effect (Batra et al., 2017; Pinto et al., 2017).

This work characterizes a new FXS hESC line, which was recently added to the NIH registry allowing for its use in United States federally–funded research. Despite a lack of FMRP, the FXS hESCs were effectively differentiated into neural rosettes and finally neurons (**Figure 4**; Eiges et al., 2007; Telias et al., 2013). This line exhibits a passage dependent silencing, including a passage-dependent methylation of the *FMR1* promoter that occurs in the absence of any neuronal differentiation (**Figure 4**). This is consistent with some published findings suggesting selection against expression of large expanded CGG repeat containing RNAs and (potentially) RAN translation products (Brykczynska et al., 2016; Zhou et al., 2016). However, it disagrees with work in the first characterized and widely used hESC FXS

line that exhibits a neuronal differentiation-dependent silencing that appears dependent on an RNA induced transcriptional silencing mechanism (Eiges et al., 2007; Colak et al., 2014). Our work does not delineate between these two possibilities, but future studies over longer time courses using stable transfection systems will be needed to determine both the sustainability of the enhanced transcription observed and the impact of enhanced production of large CGG repeat RNAs on cell viability and differentiation.

This study is complementary to a series of recent articles utilizing the CRISPR-Cas9 system to reactivate transcription from the *FMR1* locus in FXS. Two studies took a more direct approach of cutting out the repeat with the Cas9 nuclease and both achieved correction of the transcriptional silencing and a reactivation of FMRP expression (Park et al., 2016; Xie et al., 2016). More recently, a third study used a strategy more akin to our approach, targeting gRNAs to the CGG repeat and coupling that with a dCas9 fused to the active domain of the TET DNA demethylase (Liu et al., 2016, 2018). Using this approach in an iPSC line with ~500 CGG repeats, they were able to achieve both transcriptional reactivation of *FMR1* as well as at least partial recovery of FMRP expression (Liu et al., 2018). As with our work, it is intriguing that reactivation of *FMR1* transcription can occur even at a fully methylated and transcriptionally silenced locus observed in the late passage FXS hESCs (**Figure 4B**). This suggests that methylation and heterochromatization of the locus

do not preclude access of the gRNAs and dCas9 complex to the repeat sequence. Our study adds the additional element that even targeting a transcription factor to the repeat, which does not directly target the epigenetic alterations present at the locus in FXS, is sufficient to reactivate the gene. Taken together, these findings imply that the silenced CGG repeat expanded *FMR1* locus may be more dynamic than previously thought- at least in the setting of hESCs where such boundaries may be more permissive to epigenetic change. Moreover, these results imply that *FMR1* transcriptional reactivation can be achieved through multiple potentially complementary approaches.

While the dCas9-VP192 activation system in control HEK293T cells elicited relatively equivalent effects on both *FMR1* transcription and FMRP production, in hESCs with pathologic repeat expansions the impact of transcriptional upregulation on FMRP expression was significantly blunted (**Figure 7**). There are a number of potential explanations for this finding. First, the method of dCas9-VP192 complex delivery utilized in these studies (transient transfection) was different from those used in studies with dCas9-Tet1 (Viral delivery with extension of measures of FMRP synthesis for weeks after transduction). Transfection rates empirically determined in our studies in hESCs were ∼50%, meaning that any effects were diluted by the contribution of un-transfected cells. Viral delivery, especially in NPCs, is more efficient and expression is prolonged, which may explain their greater impact on both *FMR1* transcription and FMRP production. These delivery issues may also limit our ability to accurately exclude off-target effects if an insufficient number of cells were effectively transfected. Second, delivery of a transcriptional activator absent DNA demethylation may be less efficient at reactivating *FMR1* mRNA expression compared with a targeted demethylation. Direct head-to-head experiments with identical delivery mechanisms and multiple cell lines as well as evaluation for potential synergistic impacts on gene reactivation will need to be evaluated in the future.

An alternative explanation for the observed discrepancy between *FMR1* mRNA transcriptional reactivation and FMRP production could be the larger repeat size of the hESC line studied in these experiments (>800 CGG repeats). Transcribed and expanded CGG repeats elicit a significant impedance to ribosomal scanning and downstream initiation of FMRP translation (Feng et al., 1995; Chen et al., 2003; Khateb et al., 2007; Iliff et al., 2013). How large of a factor such a translational blockade might play in any transcriptional re-activation strategy is unclear. Very large un-methylated repeats that are efficiently transcribed can still produce a FXS phenotype, although some cases of methylation mosaicism and repeat length mosaicism have only modest or no clear clinical symptoms (Burman et al., 1999; Tassone et al., 2000). It may be that the underlying repeat size is the critical determinant. Most cases of unmethylated full mutation patients described to date have repeat sizes that are less than 400 CGGs and these typically have very mild if any clinical phenotypes (Pietrobono et al., 2005; Tabolacci and Chiurazzi, 2013). In cases of methylation mosaicism, somatic instability complicates data interpretation, meaning that effects on FMRP production may be cell specific (Jiraanont et al., 2017).

If transcribed repeats preclude recovery of FMRP expression in FXS patients with very large expansions, then concomitant approaches specifically targeting this translational blockade will be needed to achieve reactivation in these cases. However, given that less CGG DNA methylation, more *FMR1* mRNA transcription and more FMRP production in even a subset of cells in FXS patients all correlate with better clinical outcomes and differential responses to pharmacological agents (Nolin et al., 1994; Tassone et al., 1999; Jacquemont et al., 2011), even modest successes targeting these proximal events in pathogenesis may elicit meaningful effects on clinical phenotypes. Thus, this proof-of-principle study provides additional hope that such approaches will eventually lead to effective therapeutics in patients with FXS while also raising concerns related to the generalizability of the approach to all cases.

DATA AVAILABILITY

The datasets generated for this study can be found in the GEO database GEO identifierGSE112031 (https://www.ncbi.nlm.nih.gov/geo/query/acc.cgi?acc=GSE112031).

AUTHOR CONTRIBUTIONS

PT and JH conceived the project. JH conducted all of the experiments in HEK293T cells and all initial experiments in hESC cells. GS validated hESC experiments, did NPC and neuronal work and performed the RNA-seq experiments. GS wrote the manuscript with significant input from PT and JH. GSmith and AMR derived the UM139-2 hESC line. CR initially characterized the UM 139-2 hESC line. JP provided assistance with stem cell work. All authors edited the manuscript.

FUNDING

ACKNOWLEDGMENTS

SUPPLEMENTARY MATERIAL

The Supplementary Material for this article can be found online at: https://www.frontiersin.org/articles/10.3389/fnmol.2018.00282/full#supplementary-material

FIGURE S1 | Gene ontology analysis and pathways for WT vs. late FXS hESCs. **(A)** Graph depicting top Gene Ontology (GO) terms for the RNA-seq data comparing WT and FXS hESCs. *X*-axis shows the GO terms and *Y*-axis shows the negative log (base 10) of the *p*-values for each category. **(B)** All pathways from the WT and FXS hESC RNA-seq analysis are plotted in terms of the two types of evidence computed by iPathwayGuide using Impact Analysis (Tarca et al., 2009): over-representation on the *x*-axis (pORA-Over Representation Analysis) and the total pathway accumulation on the *y*-axis (pAcc: Accumulated perturbation of the pathway). Each pathway is represented by a single dot, with significant pathways shown in red, non-significant in black. Both *p*-values are shown in terms of their negative log (base 10) values. Yellow dot represents cancer pathways. The adjacent red dots show pathways for melanoma and breast cancer. Figure obtained from iPathwayGuide (http://www.advaitabio.com/ipathwayguide).

TABLE S1 | List of all primers used to construct sgRNA plasmids and for qPCR analysis in this study.

REFERENCES

Alpatov, R., Lesch, B. J., Nakamoto-Kinoshita, M., Blanco, A., Chen, S., Stutzer, A., et al. (2014). A chromatin-dependent role of the Fragile X mental retardation protein FMRP in the DNA damage response. *Cell* 157, 869–881. doi: 10.1016/j.cell.2014.03.040

Ascano, M. Jr., Mukherjee, N., Bandaru, P., Miller, J. B., Nusbaum, J. D., Corcoran, D. L., et al. (2012). FMRP targets distinct mRNA sequence elements to regulate protein expression. *Nature* 492, 382–386. doi: 10.1038/nature11737

Avitzour, M., Mor-Shaked, H., Yanovsky-Dagan, S., Aharoni, S., Altarescu, G., Renbaum, P., et al. (2014). *FMR1* epigenetic silencing commonly occurs in undifferentiated Fragile X-affected embryonic stem cells. *Stem Cell Reports* 3, 699–706. doi: 10.1016/j.stemcr.2014.09.001

Balboa, D., Weltner, J., Eurola, S., Trokovic, R., Wartiovaara, K., and Otonkoski, T. (2015). Conditionally stabilized dCas9 activator for controlling gene expression in human cell reprogramming and differentiation. *Stem Cell Reports* 5, 448–459. doi: 10.1016/j.stemcr.2015.08.001

Batra, R., Nelles, D. A., Pirie, E., Blue, S. M., Marina, R. J., Wang, H., et al. (2017). Elimination of toxic microsatellite repeat expansion RNA by RNA-targeting Cas9. *Cell* 170, 899–912.e10. doi: 10.1016/j.cell.2017.07.010

Bear, M. F., Huber, K. M., and Warren, S. T. (2004). The mGluR theory of Fragile X mental retardation. *Trends Neurosci.* 27, 370–377. doi: 10.1016/j.tins.2004.04.009

Berry-Kravis, E., Des Portes, V., Hagerman, R., Jacquemont, S., Charles, P., Visootsak, J., et al. (2016). Mavoglurant in Fragile X syndrome: results of two randomized, double-blind, placebo-controlled trials. *Sci. Transl. Med.* 8:321ra325. doi: 10.1126/scitranslmed.aab4109.

Berry-Kravis, E., Hagerman, R., Visootsak, J., Budimirovic, D., Kaufmann, W. E., Cherubini, M., et al. (2017). Arbaclofen in Fragile X syndrome: results of phase 3 trials. *J. Neurodev. Disord.* 9:3. doi: 10.1186/s11689-016-9181-6

Berry-Kravis, E. M., Lindemann, L., Jonch, A. E., Apostol, G., Bear, M. F., Carpenter, R. L., et al. (2017). Drug development for neurodevelopmental disorders: lessons learned from Fragile X syndrome. *Nat. Rev. Drug Discov.* 17, 280–299. doi: 10.1038/nrd.2017.221

Bhakar, A. L., Dölen, G., and Bear, M. F. (2012). The pathophysiology of Fragile X (and what it teaches us about synapses). *Annu. Rev. Neurosci.* 35, 417–443. doi: 10.1146/annurev-neuro-060909-153138

Biacsi, R., Kumari, D., and Usdin, K. (2008). SIRT1 inhibition alleviates gene silencing in Fragile X mental retardation syndrome. *PLoS Genet.* 4:e1000017. doi: 10.1371/journal.pgen.1000017

Braat, S., D'Hulst, C., Heulens, I., De Rubeis, S., Mientjes, E., Nelson, D. L., et al. (2015). The GABAA receptor is an FMRP target with therapeutic potential in Fragile X syndrome. *Cell Cycle* 14, 2985–2995. doi: 10.4161/15384101.2014.989114

Brown, V., Jin, P., Ceman, S., Darnell, J. C., O'Donnell, W. T., Tenenbaum, S. A., et al. (2001). Microarray identification of FMRP-associated brain mRNAs and altered mRNA translational profiles in Fragile X syndrome. *Cell* 107, 477–487. doi: 10.1016/s0092-8674(01)00568-2

Brown, M. R., Kronengold, J., Gazula, V. R., Chen, Y., Strumbos, J. G., Sigworth, F. J., et al. (2010). Fragile X mental retardation protein controls gating of the sodium-activated potassium channel slack. *Nat. Neurosci.* 13, 819–821. doi: 10.1038/nn.2563

Brykczynska, U., Pecho-Vrieseling, E., Thiemeyer, A., Klein, J., Fruh, I., Doll, T., et al. (2016). CGG repeat-induced *FMR1* silencing depends on the expansion size in human iPSCs and neurons carrying unmethylated full mutations. *Stem Cell Reports* 7, 1059–1071. doi: 10.1016/j.stemcr.2016.10.004

Burman, R. W., Popovich, B. W., Jacky, P. B., and Turker, M. S. (1999). Fully expanded *FMR1* CGG repeats exhibit a length- and differentiation-dependent instability in cell hybrids that is independent of DNA methylation. *Hum. Mol. Genet.* 8, 2293–2302. doi: 10.1093/hmg/8.12.2293

Ceman, S., O'Donnell, W. T., Reed, M., Patton, S., Pohl, J., and Warren, S. T. (2003). Phosphorylation influences the translation state of FMRP-associated polyribosomes. *Hum. Mol. Genet.* 12, 3295–3305. doi: 10.1093/hmg/ddg350

Chang, S., Bray, S. M., Li, Z., Zarnescu, D. C., He, C., Jin, P., et al. (2008). Identification of small molecules rescuing Fragile X syndrome phenotypes in *Drosophila*. *Nat. Chem. Biol.* 4, 256–263. doi: 10.1038/nchembio.78

Chavez, A., Scheiman, J., Vora, S., Pruitt, B. W., Tuttle, M., P R Iyer, E., et al. (2015). Highly efficient Cas9-mediated transcriptional programming. *Nat. Methods* 12, 326–328. doi: 10.1038/nmeth.3312

Cheever, A., and Ceman, S. (2009). Translation regulation of mRNAs by the Fragile X family of proteins through the microRNA pathway. *RNA Biol.* 6, 175–178. doi: 10.4161/rna.6.2.8196

Chen, E., Sharma, M. R., Shi, X., Agrawal, R. K., and Joseph, S. (2014). Fragile X mental retardation protein regulates translation by binding directly to the ribosome. *Mol. Cell* 54, 407–417. doi: 10.1016/j.molcel.2014.03.023

Chen, L. S., Tassone, F., Sahota, P., and Hagerman, P. J. (2003). The (CGG)n repeat element within the 5′ untranslated region of the *FMR1* message provides both positive and negative cis effects on *in vivo* translation of a downstream reporter. *Hum. Mol. Genet.* 12, 3067–3074. doi: 10.1093/hmg/ddg331

Cheng, A. W., Wang, H., Yang, H., Shi, L., Katz, Y., Theunissen, T. W., et al. (2013). Multiplexed activation of endogenous genes by CRISPR-on, an RNA-guided transcriptional activator system. *Cell Res.* 23, 1163–1171. doi: 10.1038/cr.2013.122

Chiurazzi, P., Pomponi, M. G., Willemsen, R., Oostra, B. A., and Neri, G. (1998). *In vitro* reactivation of the *FMR1* gene involved in Fragile X syndrome. *Hum. Mol. Genet.* 7, 109–113. doi: 10.1093/hmg/7.1.109

Coffee, B., Zhang, F., Ceman, S., Warren, S. T., and Reines, D. (2002). Histone modifications depict an aberrantly heterochromatinized *FMR1* gene in Fragile X syndrome. *Am. J. Hum. Genet.* 71, 923–932. doi: 10.1086/342931

Colak, D., Zaninovic, N., Cohen, M. S., Rosenwaks, Z., Yang, W. Y., Gerhardt, J., et al. (2014). Promoter-bound trinucleotide repeat mRNA drives epigenetic silencing in Fragile X syndrome. *Science* 343, 1002–1005. doi: 10.1126/science.1245831

Darnell, J. C., Van Driesche, S. J., Zhang, C., Hung, K. Y., Mele, A., Fraser, C. E., et al. (2011). FMRP stalls ribosomal translocation on mRNAs linked to synaptic function and autism. *Cell* 146, 247–261. doi: 10.1016/j.cell.2011.06.013

De Boulle, K., Verkerk, A. J., Reyniers, E., Vits, L., Hendrickx, J., Van Roy, B., et al. (1993). A point mutation in the FMR-1 gene associated with Fragile X mental retardation. *Nat. Genet.* 3, 31–35. doi: 10.1038/ng0193-31

de Esch, C. E., Ghazvini, M., Loos, F., Schelling-Kazaryan, N., Widagdo, W., Munshi, S. T., et al. (2014). Epigenetic characterization of the *FMR1* promoter in induced pluripotent stem cells from human fibroblasts carrying an unmethylated full mutation. *Stem Cell Reports* 3, 548–555. doi: 10.1016/j.stemcr.2014.07.013

Deng, P. Y., Rotman, Z., Blundon, J. A., Cho, Y., Cui, J., Cavalli, V., et al. (2013). FMRP regulates neurotransmitter release and synaptic information transmission by modulating action potential duration via BK channels. *Neuron* 77, 696–711. doi: 10.1016/j.neuron.2012.12.018

Dölen, G., Osterweil, E., Rao, B. S., Smith, G. B., Auerbach, B. D., Chattarji, S., et al. (2007). Correction of Fragile X syndrome in mice. *Neuron* 56, 955–962. doi: 10.1016/j.neuron.2007.12.001

Doudna, J. A., and Charpentier, E. (2014). Genome editing. The new frontier of genome engineering with CRISPR-Cas9. *Science* 346:1258096. doi: 10.1126/science.1258096

Eiges, R., Urbach, A., Malcov, M., Frumkin, T., Schwartz, T., Amit, A., et al. (2007). Developmental study of Fragile X syndrome using human embryonic stem cells derived from preimplantation genetically diagnosed embryos. *Cell Stem Cell* 1, 568–577. doi: 10.1016/j.stem.2007.09.001

Feng, Y., Gutekunst, C. A., Eberhart, D. E., Yi, H., Warren, S. T., and Hersch, S. M. (1997). Fragile X mental retardation protein: nucleocytoplasmic shuttling and association with somatodendritic ribosomes. *J. Neurosci.* 17, 1539–1547. doi: 10.1523/jneurosci.17-05-01539.1997

Feng, Y., Zhang, F., Lokey, L. K., Chastain, J. L., Lakkis, L., Eberhart, D., et al. (1995). Translational suppression by trinucleotide repeat expansion at *FMR1*. *Science* 268, 731–734. doi: 10.1126/science.7732383

Gecz, J., Gedeon, A. K., Sutherland, G. R., and Mulley, J. C. (1996). Identification of the gene FMR2, associated with FRAXE mental retardation. *Nat. Genet.* 13, 105–108. doi: 10.1038/ng0596-105

Gedeon, A. K., Baker, E., Robinson, H., Partington, M. W., Gross, B., Manca, A., et al. (1992). Fragile X syndrome without CCG amplification has an *FMR1* deletion. *Nat. Genet.* 1, 341–344. doi: 10.1038/ng0892-341

Gold, B., Radu, D., Balanko, A., and Chiang, C.-S. (2000). Diagnosis of Fragile X syndrome by Southern blot hybridization using a chemiluminescent probe: a laboratory protocol. *Mol. Diagn.* 5, 169–178. doi: 10.1054/modi.2000.9404

Hou, L., Antion, M. D., Hu, D., Spencer, C. M., Paylor, R., and Klann, E. (2006). Dynamic translational and proteasomal regulation of Fragile X mental retardation protein controls mGluR-dependent long-term depression. *Neuron* 51, 441–454. doi: 10.1016/j.neuron.2006.07.005

Hsu, P. D., Lander, E. S., and Zhang, F. (2014). Development and applications of CRISPR-Cas9 for genome engineering. *Cell* 157, 1262–1278. doi: 10.1016/j.cell.2014.05.010

Hsu, P. D., Scott, D. A., Weinstein, J. A., Ran, F. A., Konermann, S., Agarwala, V., et al. (2013). DNA targeting specificity of RNA-guided Cas9 nucleases. *Nat. Biotechnol.* 31, 827–832. doi: 10.1038/nbt.2647

Hunter, J., Rivero-Arias, O., Angelov, A., Kim, E., Fotheringham, I., and Leal, J. (2014). Epidemiology of Fragile X syndrome: a systematic review and meta-analysis. *Am. J. Med. Genet. A* 164A, 1648–1658. doi: 10.1002/ajmg.a.36511

Iliff, A. J., Renoux, A. J., Krans, A., Usdin, K., Sutton, M. A., and Todd, P. K. (2013). Impaired activity-dependent FMRP translation and enhanced mGluR-dependent LTD in Fragile X premutation mice. *Hum. Mol. Genet.* 22, 1180–1192. doi: 10.1093/hmg/dds525

Jacquemont, S., Curie, A., des Portes, V., Torrioli, M. G., Berry-Kravis, E., Hagerman, R. J., et al. (2011). Epigenetic modification of the *FMR1* gene in Fragile X syndrome is associated with differential response to the mGluR5 antagonist AFQ056. *Sci. Transl. Med.* 3:64ra61. doi: 10.1126/scitranslmed.3001708

Jiraanont, P., Kumar, M., Tang, H. T., Espinal, G., Hagerman, P. J., Hagerman, R. J., et al. (2017). Size and methylation mosaicism in males with Fragile X syndrome. *Expert Rev. Mol. Diagn.* 17, 1023–1032. doi: 10.1080/14737159.2017.1377612

Khateb, S., Weisman-Shomer, P., Hershco-Shani, I., Ludwig, A. L., and Fry, M. (2007). The tetraplex (CGG)n destabilizing proteins hnRNP A2 and CBF-A enhance the *in vivo* translation of Fragile X premutation mRNA. *Nucleic Acids Res.* 35, 5775–5788. doi: 10.1093/nar/gkm636

Kim, M., Bellini, M., and Ceman, S. (2009). Fragile X mental retardation protein FMRP binds mRNAs in the nucleus. *Mol. Cell. Biol.* 29, 214–228. doi: 10.1128/MCB.01377-08

Knight, S. J. L., Flannery, A. V., Hirst, M. C., Campbell, L., Christodoulou, Z., Phelps, S. R., et al. (1993). Trinucleotide repeat amplification and hypermethylation of a CpG island in FRAXE mental retardation. *Cell* 74, 127–134. doi: 10.1016/0092-8674(93)90300-f

Korb, E., Herre, M., Zucker-Scharff, I., Gresack, J., Allis, C. D., and Darnell, R. B. (2017). Excess translation of epigenetic regulators contributes to Fragile X syndrome and is alleviated by Brd4 inhibition. *Cell* 170, 1209.e20–1223.e20. doi: 10.1016/j.cell.2017.07.033

Kumari, D., and Usdin, K. (2016). Sustained expression of *FMR1* mRNA from reactivated Fragile X syndrome alleles after treatment with small molecules

that prevent trimethylation of H3K27. *Hum. Mol. Genet.* 25, 3689–3698. doi: 10.1093/hmg/ddw215

Langmead, B., Trapnell, C., Pop, M., and Salzberg, S. L. (2009). Ultrafast and memory-efficient alignment of short DNA sequences to the human genome. *Genome Biol.* 10:R25. doi: 10.1186/gb-2009-10-3-r25

Lee, H. Y., Ge, W. P., Huang, W., He, Y., Wang, G. X., Rowson-Baldwin, A., et al. (2011). Bidirectional regulation of dendritic voltage-gated potassium channels by the Fragile X mental retardation protein. *Neuron* 72, 630–642. doi: 10.1016/j.neuron.2011.09.033

Ligsay, A., Van Dijck, A., Nguyen, D. V., Lozano, R., Chen, Y., Bickel, E. S., et al. (2017). A randomized double-blind, placebo-controlled trial of ganaxolone in children and adolescents with Fragile X syndrome. *J. Neurodev. Disord.* 9:26. doi: 10.1186/s11689-017-9207-8

Liu, X. S., Wu, H., Ji, X., Stelzer, Y., Wu, X., Czauderna, S., et al. (2016). Editing DNA methylation in the Mammalian genome. *Cell* 167, 233.e17–247.e17. doi: 10.1016/j.cell.2016.08.056

Liu, X. S., Wu, H., Krzisch, M., Wu, X., Graef, J., Muffat, J., et al. (2018). Rescue of Fragile X syndrome neurons by DNA methylation editing of the *FMR1* gene. *Cell* 172, 979.e6–992.e6. doi: 10.1016/j.cell.2018.01.012

Long, C., Amoasii, L., Mireault, A. A., McAnally, J. R., Li, H., Sanchez-Ortiz, E., et al. (2016). Postnatal genome editing partially restores dystrophin expression in a mouse model of muscular dystrophy. *Science* 351, 400–403. doi: 10.1126/science.aad5725

Lucá, R., Averna, M., Zalfa, F., Vecchi, M., Bianchi, F., Fata, G. L., et al. (2013). The Fragile X protein binds mRNAs involved in cancer progression and modulates metastasis formation. *EMBO Mol. Med.* 5, 1523–1536. doi: 10.1002/emmm.201302847

Malter, H. E., Iber, J. C., Willemsen, R., de Graaff, E., Tarleton, J. C., Leisti, J., et al. (1997). Characterization of the full Fragile X syndrome mutation in fetal gametes. *Nat. Genet.* 15, 165–169. doi: 10.1038/ng0297-165

Michalon, A., Sidorov, M., Ballard, T. M., Ozmen, L., Spooren, W., Wettstein, J. G., et al. (2012). Chronic pharmacological mGlu5 inhibition corrects Fragile X in adult mice. *Neuron* 74, 49–56. doi: 10.1016/j.neuron.2012.03.009

Nalavadi, V. C., Muddashetty, R. S., Gross, C., and Bassell, G. J. (2012). Dephosphorylation-induced ubiquitination and degradation of FMRP in dendrites: a role in immediate early mGluR-stimulated translation. *J. Neurosci.* 32, 2582–2587. doi: 10.1523/jneurosci.5057-11.2012

Nelson, C. E., Hakim, C. H., Ousterout, D. G., Thakore, P. I., Moreb, E. A., Rivera, R. M. C., et al. (2016). *In vivo* genome editing improves muscle function in a mouse model of Duchenne muscular dystrophy. *Science* 351, 403–407. doi: 10.1126/science.aad5143

Nolin, S. L., Glicksman, A., Houck, G. E. Jr., Brown, W. T., and Dobkin, C. S. (1994). Mosaicism in Fragile X affected males. *Am. J. Med. Genet.* 51, 509–512. doi: 10.1002/ajmg.1320510444

Oberlé, I., Rousseau, F., Heitz, D., Kretz, C., Devys, D., Hanauer, A., et al. (1991). Instability of a 550-base pair DNA segment and abnormal methylation in Fragile X syndrome. *Science* 252, 1097–1102. doi: 10.1126/science.252.5009.1097

Park, C. Y., Sung, J. J., Choi, S. H., Lee, D. R., Park, I. H., and Kim, D. W. (2016). Modeling and correction of structural variations in patient-derived iPSCs using CRISPR/Cas9. *Nat. Protoc.* 11, 2154–2169. doi: 10.1038/nprot.2016.129

Perez-Pinera, P., Kocak, D. D., Vockley, C. M., Adler, A. F., Kabadi, A. M., Polstein, L. R., et al. (2013). RNA-guided gene activation by CRISPR-Cas9-based transcription factors. *Nat. Methods* 10, 973–976. doi: 10.1038/nmeth.2600

Pieretti, M., Zhang, F. P., Fu, Y. H., Warren, S. T., Oostra, B. A., Caskey, C. T., et al. (1991). Absence of expression of the FMR-1 gene in Fragile X syndrome. *Cell* 66, 817–822. doi: 10.1016/0092-8674(91)90125-i

Pietrobono, R., Tabolacci, E., Zalfa, F., Zito, I., Terracciano, A., Moscato, U., et al. (2005). Molecular dissection of the events leading to inactivation of the *FMR1* gene. *Hum. Mol. Genet.* 14, 267–277. doi: 10.1093/hmg/ddi024

Pinto, B. S., Saxena, T., Oliveira, R., Méndez-Gómez, H. R., Cleary, J. D., Denes, L. T., et al. (2017). Impeding transcription of expanded microsatellite repeats by deactivated Cas9. *Mol. Cell* 68, 479–490. doi: 10.1016/j.molcel.2017.09.033

Renoux, A. J., Carducci, N. M., Ahmady, A. A., and Todd, P. K. (2014). Fragile X mental retardation protein expression in Alzheimer's disease. *Front. Genet.* 5:360. doi: 10.3389/fgene.2014.00360

Santoro, M. R., Bray, S. M., and Warren, S. T. (2012). Molecular mechanisms of Fragile X syndrome: a twenty-year perspective. *Annu. Rev. Pathol.* 7, 219–245. doi: 10.1146/annurev-pathol-011811-132457

Shi, Y., Kirwan, P., and Livesey, F. J. (2012). Directed differentiation of human pluripotent stem cells to cerebral cortex neurons and neural networks. *Nat. Protoc.* 7, 1836–1846. doi: 10.1038/nprot.2012.116

Tabolacci, E., and Chiurazzi, P. (2013). Epigenetics, Fragile X syndrome and transcriptional therapy. *Am. J. Med. Genet. A* 161A, 2797–2808. doi: 10.1002/ajmg.a.36264

Tabolacci, E., Palumbo, F., Nobile, V., and Neri, G. (2016). Transcriptional reactivation of the *FMR1* Gene. A possible approach to the treatment of the Fragile X Syndrome. *Genes* 7:E49. doi: 10.3390/genes7080049

Tarca, A. L., Draghici, S., Khatri, P., Hassan, S. S., Mittal, P., Kim, J., et al. (2009). A novel signaling pathway impact analysis. *Bioinformatics* 25, 75–82. doi: 10.1093/bioinformatics/btn577

Tassone, F., Hagerman, R. J., Chamberlain, W. D., and Hagerman, P. J. (2000). Transcription of the *FMR1* gene in individuals with Fragile X syndrome. *Am. J. Med. Genet.* 97, 195–203. doi: 10.1002/1096-8628(200023)97:3<195::AID-AJMG1037>3.0.CO;2-R

Tassone, F., Hagerman, R. J., Ikle, D. N., Dyer, P. N., Lampe, M., Willemsen, R., et al. (1999). FMRP expression as a potential prognostic indicator in Fragile X syndrome. *Am. J. Med. Genet.* 84, 250–261. doi: 10.1002/(sici)1096-8628(19990528)84:3<250::aid-ajmg17>3.3.co;2-w

Tassone, F., Iong, K. P., Tong, T. H., Lo, J., Gane, L. W., Berry-Kravis, E., et al. (2012). *FMR1* CGG allele size and prevalence ascertained through newborn screening in the United States. *Genome Med.* 4:100. doi: 10.1186/gm401

Telias, M., Segal, M., and Ben-Yosef, D. (2013). Neural differentiation of Fragile X human embryonic stem cells reveals abnormal patterns of development despite successful neurogenesis. *Dev. Biol.* 374, 32–45. doi: 10.1016/j.ydbio.2012.11.031

Trapnell, C., Hendrickson, D. G., Sauvageau, M., Goff, L., Rinn, J. L., and Pachter, L. (2013). Differential analysis of gene regulation at transcript resolution with RNA-seq. *Nat. Biotechnol.* 31, 46–53. doi: 10.1038/nbt.2450

Trapnell, C., Pachter, L., and Salzberg, S. L. (2009). TopHat: discovering splice junctions with RNA-Seq. *Bioinformatics* 25, 1105–1111. doi: 10.1093/bioinformatics/btp120

Usdin, K., and Kumari, D. (2015). Repeat-mediated epigenetic dysregulation of the *FMR1* gene in the Fragile X-related disorders. *Front. Genet.* 6:192. doi: 10.3389/fgene.2015.00192

Wang, H., La Russa, M., and Qi, L. S. (2016). CRISPR/Cas9 in genome editing and beyond. *Annu. Rev. Biochem.* 85, 227–264. doi: 10.1146/annurev-biochem-060815-014607

Xie, N., Gong, H., Suhl, J. A., Chopra, P., Wang, T., and Warren, S. T. (2016). Reactivation of *FMR1* by CRISPR/Cas9-mediated deletion of the expanded CGG-repeat of the Fragile X Chromosome. *PLoS One* 11:e0165499. doi: 10.1371/journal.pone.0165499

Zalfa, F., Panasiti, V., Carotti, S., Zingariello, M., Perrone, G., Sancillo, L., et al. (2017). The Fragile X mental retardation protein regulates tumor invasiveness-related pathways in melanoma cells. *Cell Death Dis.* 8:e3169. doi: 10.1038/cddis.2017.521

Zhou, Y., Kumari, D., Sciascia, N., and Usdin, K. (2016). CGG-repeat dynamics and *FMR1* gene silencing in Fragile X syndrome stem cells and stem cell-derived neurons. *Mol. Autism* 7:42. doi: 10.1186/s13229-016-0105-9